Computational Fluid Dynamics Modelling and Simulation for Angulated Neck of Abdominal Aortic Aneurysm

Yousif Ali Yousif Al-Gabri

A Thesis Submitted in Fulfillment of the Requirements for the Degree of Master of Science in Biomedical Engineering Prince of Songkla University 2018

Computational Fluid Dynamics Modelling and Simulation for Angular Neck of Abdominal Aortic Aneurysm

Yousif Ali Yousif Al-Gabri

**A Thesis Submitted in Fulfillment of the Requirements for the
Degree of Master of Science in Biomedical Engineering
Prince of Songkla University
2018**

Thesis Title   Computational Fluid Dynamics Modelling and Simulation for Angulated Neck of Abdominal Aortic Aneurysm

Author   Mr. Yousif Ali Yousif Al-Gabri

Major Program   Biomedical Engineering

Major Advisor

…………………………………
(Asst. Prof. Dr. Surapong Chatpun)

Examining Committee:

…………………….……Chairperson
(Assoc. Prof. Dr. Boonchai Lertnuwat)

………………………….Committee
(Asst. Prof. Dr. Chayut Nuntadusit)

………………..…………..Committee
(Dr. Somyot Chirasatitsin)

………………….…..……..Committee
(Asst. Prof. Dr. Surapong Chatpun)

The Graduate School, Prince of Songkla University, has approved this thesis as fulfillment of the requirements for the Master of Science Degree in Biomedical Engineering

…………………………………………….
(Prof. Dr. Damrongsak Faroongsarng)
Dean of Graduate School

This is to certify that the work here submitted is the result of the candidate's own investigations. Due acknowledgement has been made of any assistance received.

…………………....…Signature

(Asst. Prof. Dr. Surapong Chatpun)

Major Advisor

…………………........Signature

(Mr. Yousif Ali Yousif Al-Gabri)

Candidate

I hereby certify that this work has not been accepted in substance for any degree and is not being currently submitted in candidature for any degree.

………………….......Signature

(Mr. Yousif Ali Yousif Al-Gabri)

Candidate

Thesis title   Computational Fluid Dynamics Modelling and Simulation for Angulated Neck of Abdominal Aortic Aneurysm

Author   Mr. Yousif Ali Yousif Al-Gabri

Major Program   Biomedical Engineering

Academic year   2017

Abstract

An abdominal aortic aneurysm (AAA) is one of serious pathologies of cardiovascular diseases. This disease is defined as a localized expansion of the abdominal aorta. A normal size of a healthy artery is estimated between 1.5 and 2.4 cm based on several categories such as age, gender, and body weight. The rupture occurs if there is an increase in the aneurysm sac diameter up to 3.0 cm or if the aneurysm keeps growing or is not treated. Proximal neck angulation of AAA is believed to influence the hemodynamic changes and wall shear stress (WSS) within AAAs. This study aimed to investigate the impact of AAA angulation on the hemodynamic parameters such as flow behaviours, wall shear stress (WSS) and pressure in two different models; 3D constructed models and patient-specific geometry of angulated neck of AAA by implementing computational fluid dynamics (CFD). In this work, the 3D constructed angulated neck of AAA models were constructed using SolidWorks software, while the patient-specific AAA geometry was reconstructed from computed tomography images using Mimics software. The steady-state condition was performed for the simulation of 3D constructed models. On the other hands, the patient-specific geometry was modelled as unsteady flow. Blood was assumed as incompressible, homogenous, and Newtonian fluid. The outflow pressure was set at the outlets. Aorta wall was assumed as rigid and no-slip. The simulations were performed by using ANSYS Fluent software. The findings from the 3D constructed models indicated that max velocity which formed as a thin bar within the aneurysm is gradually increasing across the four-angulated neck abdominal aortas, this occurs because of the increase of the degree of angulated neck of AAA, while the results of patient-specific simulation showed that the blood flowing through severe bending of angular neck leads to high

turbulence and asymmetry of flows within the aneurysm sac resulting in blood recirculation and high wall shear stress (WSS) near the AAA neck and on surface of aneurysm sac. However, the results for both cases have confirmed that there is a vital impact on the velocity flow field and WSS due to the angulated neck. In conclusion, this study explained and showed flow behaviours and WSS progression within high angulated neck of AAA in both studies of steady-state and transient conditions in the idealized and the realistic angulated neck of AAA models. Furthermore, it can be seen that the CFD technique has high performance in investigating and explaining the hemodynamic changes for angulated neck of abdominal aortic aneurysm which can be used as an extra tool to assist clinicians to understand the flow behaviour and manage for the clinical intervention.

Keywords: Cardiovascular disease, Angulated neck, Abdominal aortic aneurysm, Computational fluid dynamics, Computed tomography, Patient-specific geometry

Acknowledgements

A huge and heartfelt thank you to the following people who have made this master's degree project come to life:

To my advisor, Asst. Prof. Dr. Surapong Chatpun for guidance, advice, support and inspiration throughout this journey.

I am grateful to Dr. Sorracha Rookaphan (Tong), MD and Mr. Sumrit Ruangchan (Radiology department, Faculty of Medicine, PSU) for providing us with patients CT images that used in this study and for their continuous support.

To Assoc. Prof. Dr. Boonchai Lertnuwa (Chairperson), Asst. Prof. Dr. Chayut Nuntadusit, and Dr. Somyot Chirasatitsin, my thesis defense committee for reading everything and for telling me their constructive opinions and valuable suggestions.

Thanks also to IBME academicians, staffs, and students for their continued motivation and support.

To TEH-AC scholarship and graduate school, Prince of Songkla University for the generous financial support to complete this degree.

Yousif A. Al-Gabri

Dedication

This thesis is dedicated to my dearest parents, my wonderful brothers and sisters, my wonderful friends and beloved ones. And, to my teachers and lecturers in all my educational levels.

Table of Contents

List of Tables

List of Figures

List of Abbreviations

3D   Three-dimensional

AAAs   Abdominal aortic aneurysms

CAD   Computer-aided design

CFD   Computational fluid dynamics

CT   Computed tomography

CVD   Cardiovascular disease

DICOM   Digital Imaging and Communication in Medicine

EVAR   Endovascular aortic aneurysm repair

ILT   Intraluminal thrombus

Re   Reynolds number

ROI   Region of Interests

SST   Shear-Stress Transport

STL   Stereolithography

UDF   User-defined function

WSS   Wall shear stress

List of Papers and Proceedings

Yousif A. Algabri, Sorracha Rookkapan, Vera Gramina, Daniel M. Espino, and Surapong Chatpun. Computational study on hemodynamic changes in patient-specific proximal neck angulation of abdominal aortic aneurysm with time-varying velocity, (Submitted to Arabian Journal for Science and Engineering)

Algabri Y A, Rookkapan S, Chatpun S. Three-dimensional finite volume modelling of blood flow in simulated angular neck abdominal aortic aneurysm. IOP Conf Ser Mater Sci Eng. 2017 Sep;243(1):12003.

Yousif Algabri <algabriyousif80@gmail.com>

AJSE-D-18-02776 - Submission Notification to co-author

1 message

Arabian Journal for Science and Engineering (AJSE) <em@editorialmanager.com>   Sun, Jun 24, 2018 at 11:18 AM
Reply-To: "Arabian Journal for Science and Engineering (AJSE)" <ranje.natarajan@springer.com>
To: Yousif A Algabri <algabriyousif80@gmail.com>

Re: "Computational study on hemodynamic changes in patient-specific proximal neck angulation of abdominal aortic aneurysm with time-varying velocity"
Full author list: Yousif A Algabri, BEng; Sorracha Rookkapan, M.D.; Vera Gramigna, Ph.D.; Daniel M Espino, Ph.D.; Surapong Chatpun, Ph.D.

Dear Mr. Algabri,

We have received the submission entitled: "Computational study on hemodynamic changes in patient-specific proximal neck angulation of abdominal aortic aneurysm with time-varying velocity" for possible publication in Arabian Journal for Science and Engineering, and you are listed as one of the co-authors.

The manuscript has been submitted to the journal by Dr. Dr. Surapong Chatpun who will be able to track the status of the paper through his/her login.

If you have any objections, please contact the editorial office as soon as possible. If we do not hear back from you, we will assume you agree with your co-authorship.

Thank you very much.

With kind regards,

Springer Journals Editorial Office
Arabian Journal for Science and Engineering

Summary of Contents

1. Introduction

1.1 *Cardiovascular system*

As widely known that the cardiovascular system in human body contains of several organs such as heart, blood vessels, and lymphatic vessels. The common basic roles of this system are to transport the nutrients, and oxygen to control body temperature and to eliminate waste (1). The pulmonary, systemic, and coronary circulations are the three major subsystems in cardiovascular. The pulmonary circulation carries blood to the lungs capillaries. The systemic circulation delivers blood to all body tissues. The coronary circulation is the heart blood supplier. The demands of oxygen and nutrients in body increase during performing daily activities and exercises which influence the living cells system reactions, that demands the needs of the heart. Furthermore, the arteries have the ability to generate more permanent changes in the size and shapes at their walls, this process is known as remodeling. Therefore, the failure of some arterial system functions might occur whether because of disease or other biological factors. Thus, this failure causes a part of arteries wall to enlarge or expand and this change is so-called aneurysm (2).

1.2 *Abdominal aortic aneurysm*

Aneurysm is defined as an enlargement or swelling of vessels, in another word, a bulging or ballooning the wall of blood vessel. The two common locations that aneurysm occurs are at the abdominal and intracranial aorta as well as this pathology can exist in other blood vessels (3). The aortic aneurysm usually grows in the abdominal aorta below the kidney and between the iliac bifurcation and the renal arteries (4). Therefore, this type of aneurysms is named abdominal aortic aneurysms or in short form AAA, with at least a diameter of 30 mm or about 1.5 times the normal size of aorta (5). AAA is one of the cardiovascular diseases (CVDs) that causes about 90% mortality rate, if it ruptured (6). Figure 1a shows location and differences between normal and dilated abdominal aorta (7). Abdominal aortic aneurysms (AAAs) are formed due to

several mechanisms including, inflammation of immune responses and aortic wall degradation, which are affected by molecular genetics (8,9).

1.3 *Risk factors*

There are several indicators of aneurysm rupture, for instance; dizziness, sudden abdomen pain, clammy and wet skin, and increasing of heart rate (2). The rupture of aneurysm is such a dangerous illness that contributes 65% to 85% of mortality rate, where almost have of these mortality cases happen before even admitting to the surgery.

The numerous studies that conducted on the prediction of rupture and its risks, have proposed several possible AAA rupture factors (8,10–14). These factors are asymmetry flow index, male gender, age, aortic wall stiffness, mechanical stress, aneurysm growth rate, intraluminal thrombus (ILT), smoking, hypertension and high cholesterol. It was reported that men over 60 years old are more expected to have AAAs six times than women with similar age (15,16). however, the reasons for these gender variances still unclear. Cigarette smoking and hypertriton are ranked as leading risk factors for cardiovascular disease and they cause stiffening to the arterial walls (17–20). The existence of ILT effects the degradation of proteolytic of the primary aneurysmal wall part (21). Nevertheless, the relationship between ILT and rupture has not yet clarified. However, morphologies such as aortic neck angulation related to adverse events and outcome after endovascular abdominal aortic aneurysm repair have less attention (22).

1.4 *Angulated Neck of Abdominal Aortic Aneurysm*

Aortic neck angulation was defined as the bending of the aorta between the renal arteries and proximal neck the aneurysm (22) as shown in Figure 1b. Nearly 35% of men and 60% of women are ineligible for endovascular aortic aneurysm repair (EVAR) due to a complex aneurysm morphology such as a short aortic neck, and the angulation of iliac bifurcation arteries that affect the AAA hemodynamic and undoubtedly contribute to the wall shear stresses (23–25). These morphologies were mostly overlooked in the past, while they significantly contribute to the risk of AAA rupture.

There are few studies that have considered the influence of these factors towards the aneurysmal aorta disease (26–32).

a   b
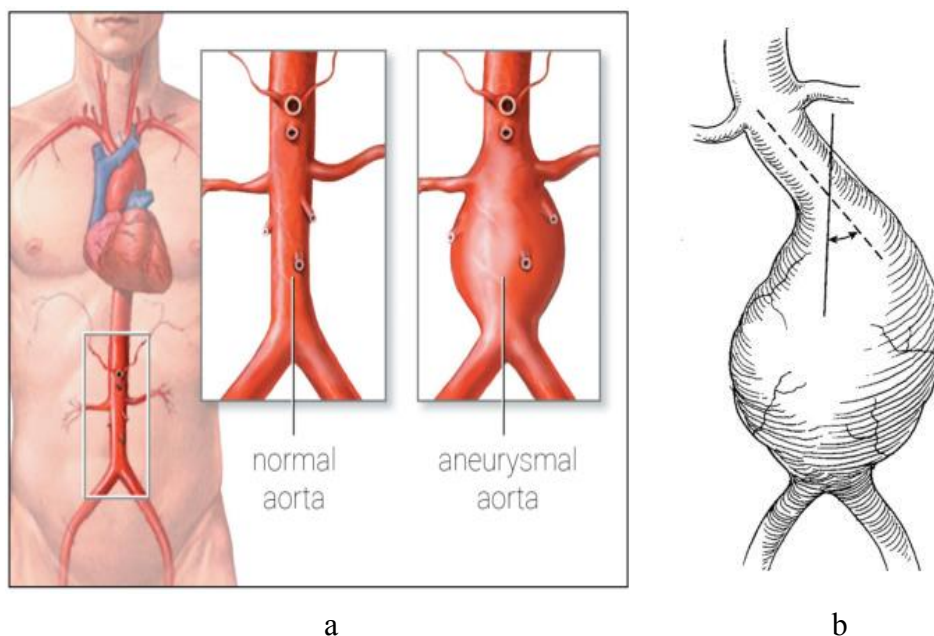
Figure 1:a: Abdominal aorta, b: location and shape of angular neck of AAA.

1.5 *Computational fluid dynamics*

Computational fluid dynamics (CFD) is progressively implemented in the applications of cardiovascular medicine that helps to investigate and solve various complicated physiological fluid flows and demonstrating their potentials (33). Generally, in clinical implementations, CFD is used for two various aims. The first aim is to understand the wide-range of several interventions and devices which can be used for aneurysm treatment and how the responds of blood flow become. This comprehension may drive to improve the designs of these devices and to make considerable choices among different possible options for suitable treatment (34,35). The second aim for applying CFD in clinical applications is to distinguish the parameters of hemodynamic and utilize these to specify the areas that are more likely to grow or form the aneurysm remodeling at the wall of artery as a result (36,37).

2. Objectives

Initially, to maintain the project's scope and its general direction within clear boundaries, specific and well-designed objectives are addressed as following.

- To study the flow patterns and behaviors in the angulated neck of abdominal aortic aneurysm with a patient's specific model using computational fluid dynamics.
- To determine hemodynamic parameters (i.e. velocity, pressure, wall shear stress) in the angulated neck of abdominal aortic aneurysm with a patient's specific model using computational fluid dynamics.

3. Materials and Methods

3.1 Geometries / Flow domain

In this study, two types of geometry reconstructions of angulated neck AAA were used for this numerical simulation. Three-dimensional (3D) simulated geometries were constructed from the scratch by using computer-aided design software ((Solid Works Corp, Concord, MA). On the other hand, patient-specific geometry was reconstructed from acquired computed tomography (CT) images as will be explained in 3.1.2 section. The 3D constructed geometry and the patient-specific geometry of angulated neck AAA are treated individually. Figure 2 illustrates the workflow for overview of this study design.
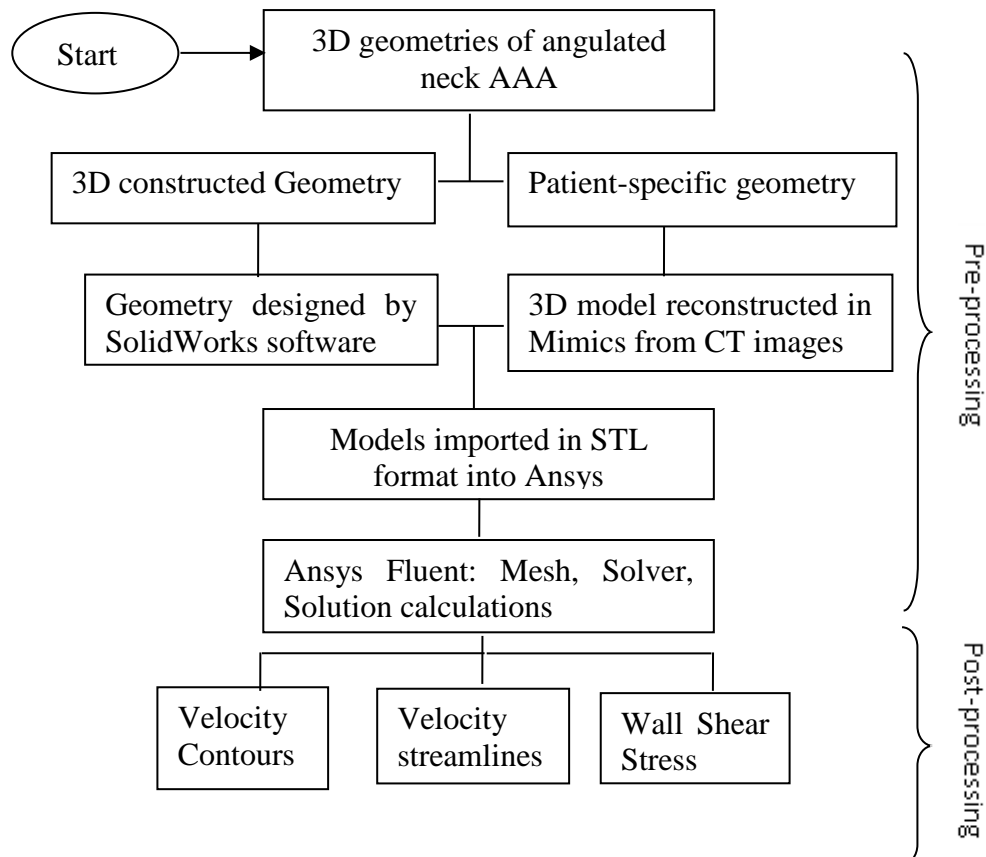
Figure 2: Flowchart for overall workflow of study methodology.

3.1.1   3D Constructed Geometry

The geometries shown in Figure 3 based on a shape of fusiform for idealized angulated abdominal aortic aneurysm (AAA) of a patient-specific. The models were constructed using SolidWorks software. The aneurysm diameter size selected is representing an average risk of rupture with 5.5 cm. The four models were designed with similar measurements and concepts and for both inlets and outlets. The diameter of the inlet is 2.0 cm while for outlets were 1.0 cm and 1.1 cm. The difference was in the angulated neck (θ) of aortic aneurysm which exactly set with a raise of 10°. These angles are 60°, 70°, 80° and 90°.

| Aortic neck | Aortic neck | Aortic neck | Aortic neck |
| angle: 60° | angle: 70° | angle: 80° | angle: 90° |
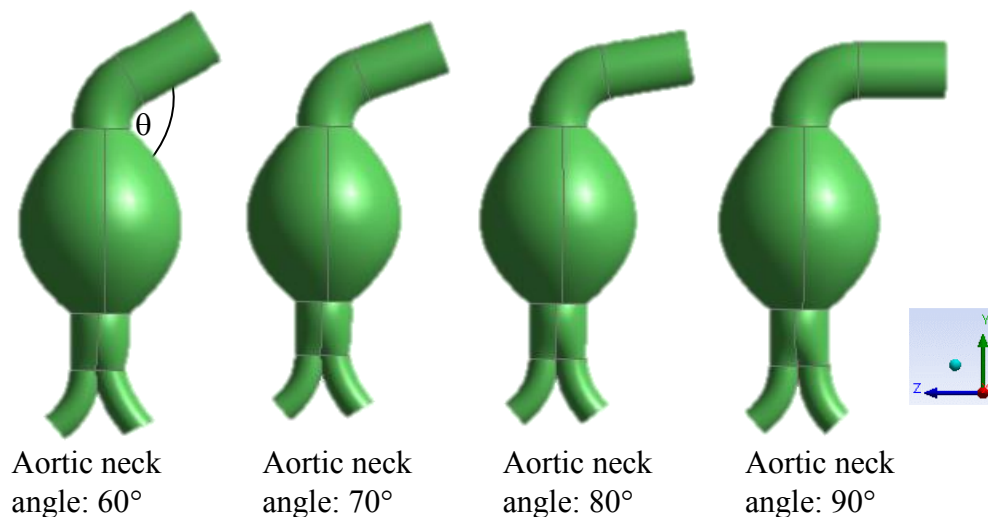
Figure 3: Geometry of AAA with varying aortic neck angulation.

3.1.2   Patient-specific Geometry

The patient-specific geometry was reconstructed from acquired CT images based on specific criteria (23,38,39) as illustrated in Table 1. These images were obtained from radiology department under the approval of Faculty of Medicine Ethics Committee, Prince of Songkla University with reference number REC.61-010-25-2 as attached in the Appendices. The CT images were obtained in a DICOM format by AQUILION PRIME (Toshiba, Japan) modality as described in Table 2. Therefore, the Three-dimensional (3D) smoothed model was generated from DICOM files by using the commercial medical imaging software Mimics v18.0 (Materialise, Belgium) are presented in figure 4. These segmentations and reconstructions process are; 4(a) CT

image obtained for the whole aorta, 4(b) the thresholding mask for aorta in the axial, coronal and sagittal view, and 4(c) 3D geometry for AAA after reconstruction. However, the patient information is detailed in Table 3.

Table 1:Inclusion criteria of patient-specific model with angulated neck of AAA.

No of Patients	Gender	Max D_{AAA}[1] (cm)	Age (yrs old)	Cigarette Use	Angle Range	CD[2]
1	Male	5.6	74	No	79°	No

Table 2: Modality information and image specifications.

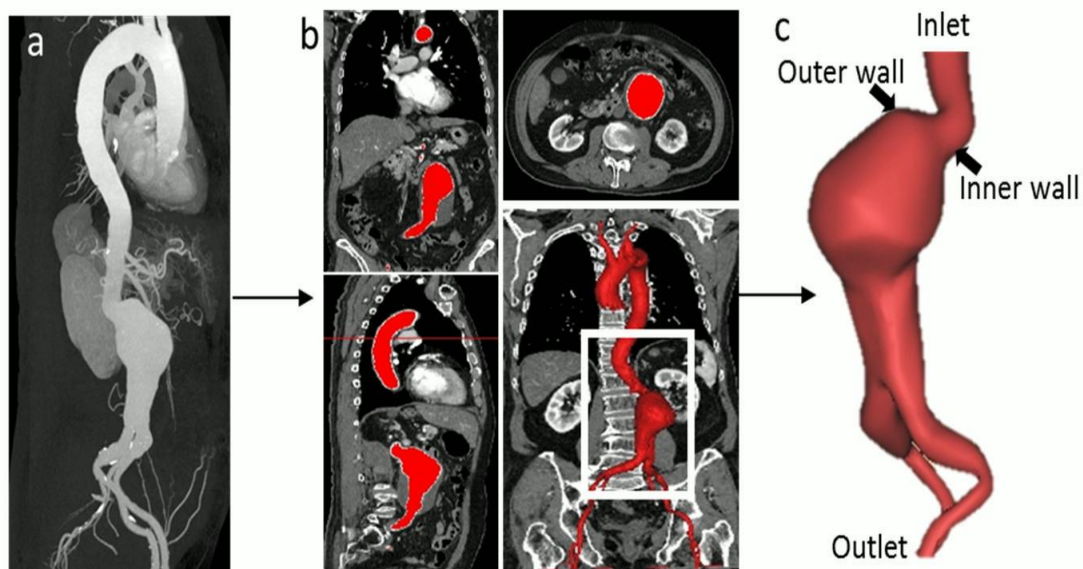| Modality	Manufacturer	Model's name	Pixel spacing	Rows/Columns	Slice thickness (mm)
CT	Toshiba	Acquilion PRIME	0.683/0.683	512/512	3

Figure 4: Segmentations and reconstructions process.

---

[1] Diameter of AAA

[2] Concomitant Disease

Table 3: Patient demographics and geometrics information.

Patient's information	
Gender	Male
Age, years	74
Weight	65
Height	158
Inflow inlet diameter (mm)	25
Proximal Neck diameter (mm)	20
Infrarenal Neck length (mm)	25
Aneurysm length (mm)	68
Aneurysm diameter (mm)	56
Distal left iliac diameter (mm)	8
Distal right iliac diameter (mm)	8
Angle at Proximal neck	79º
whole model length (mm)	258.06

3.2 Mesh

The concepts of meshing are to divide a certain model into several small elements or cells. The generation of mesh, and ratio of refinement of grid, are affected by particular factors such model design and quality. The mesh size and time-steps need to be sufficiently refined in order to capture the significant hemodynamic behavior of modelled domain, however without high refinement which requires solution time and computational resource (33).

3.2.1   3D Constructed Geometry

The geometries in Figure 3 were meshed using ANSYS Workbench v16.2 (ANSYS Inc., USA). The advanced size function was adjusted to fine both proximity and curvature because the geometries were little complex. Moreover, this feature increased the density of mesh at curved and narrow locations. The mesh independency study was performed, and the results are presented in Table 4. Therefore, based on Table 4, the graph in Figure 5 was plotted to compare between the maximum velocity and $\log_{10}$(element number) for each mesh test. Another indicator used for testing the mesh quality was obtaining the skewness values. For these models mesh, the maximum skewness was range between 0.45 to 0.53 for all meshes.

Table 4: The maximum velocity for each mesh test.

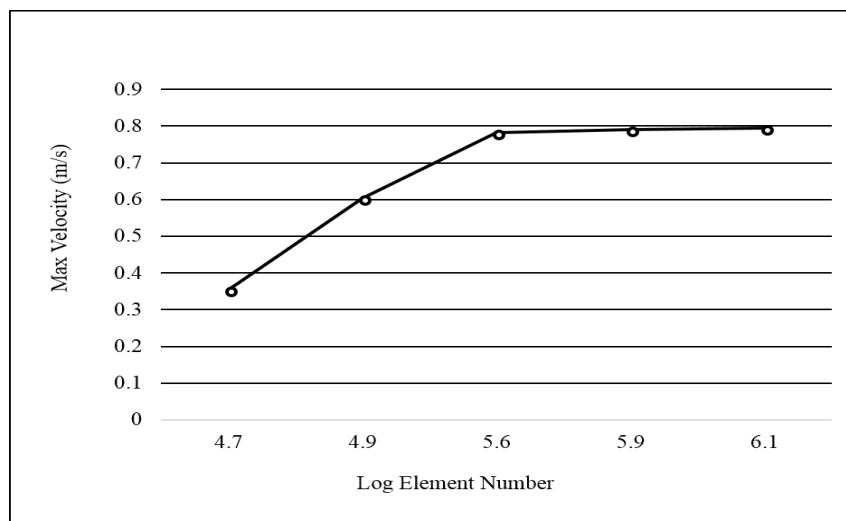| Numbers of elements	Max Velocity (m/s)
55,304	0.354813
71,379	0.603933
391,306	0.781538
972,832	0.790418
1,029,702	0.794772

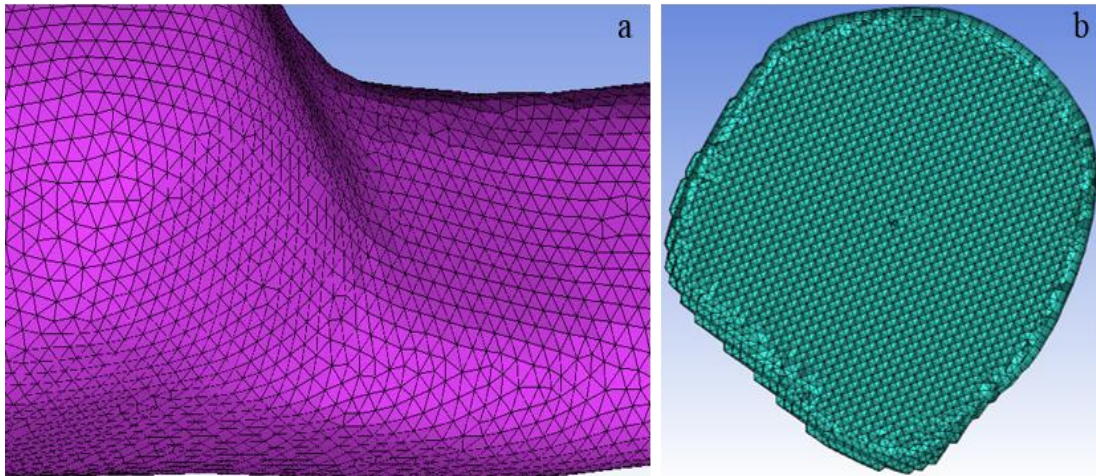Figure 5: Log element number vs. Max velocity for tested geometry.

Figure 6: Grid view of the patient-specific geometry surface mesh.

3.2.2 Patient-specific Geometry

The geometry was meshed by using the Octree method in ANSYS ICEM v16.2 (ANSYS Inc., USA) for tetrahedral meshing. Five prism boundary layers near the aorta wall with a 0.1 thickness of first layer at the inlet. Quality and smoothing checks were repeatedly performed to ensure a satisfactory mesh. A grid-size independency study was performed using a ± 2.5% for peak velocity as the key criterion. The final mesh totally had 2,077,498 elements. Figure 6a illustrates the triangular grid elements on surface while Figure 6b represents a cross-section area at the middle of aneurysm sac.

3.3 Boundary conditions

3.3.1 3D Constructed Geometry

The flow was simulated as a steady-state condition. A velocity with 0.28 m/s was set as inlet, and outlet pressure was set to zero. The abdominal aortic walls were considered as a rigid and no-slip boundary condition (40).

3.3.2 Patient-specific Geometry

The flow in this case was treated as a transient flow, which represents the nature of blood flow (41). In this case, a pulsatile velocity waveform of one cardiac cycle and a magnitude between 0 and 0.3 m/s was imposed at the aortic inlet as a user-defined

function (UDF) file, refer to Appendices. The inlet velocity waveform as shown in Figure 7: ; (a) peak systole at 0.25 s; (b) early diastole 0.55 s; (c) mid diastole 0.70 s; and (d) late diastole 0.94 s was reproduced from Rissland *et al*.(42) and Olufsen *et al*. (43) as presented in Figure 8. The arterial tree in Figure 8a shows the areas of obtained velocity which represented by letters and velocity measured at abdominal aorta was plotted in Figure 8b. The outlet boundary condition was set at both iliac arteries with a fully developed outflow zero diffusion flux (23,44). And the abdominal aortic walls were considered as a rigid and no-slip boundary condition.
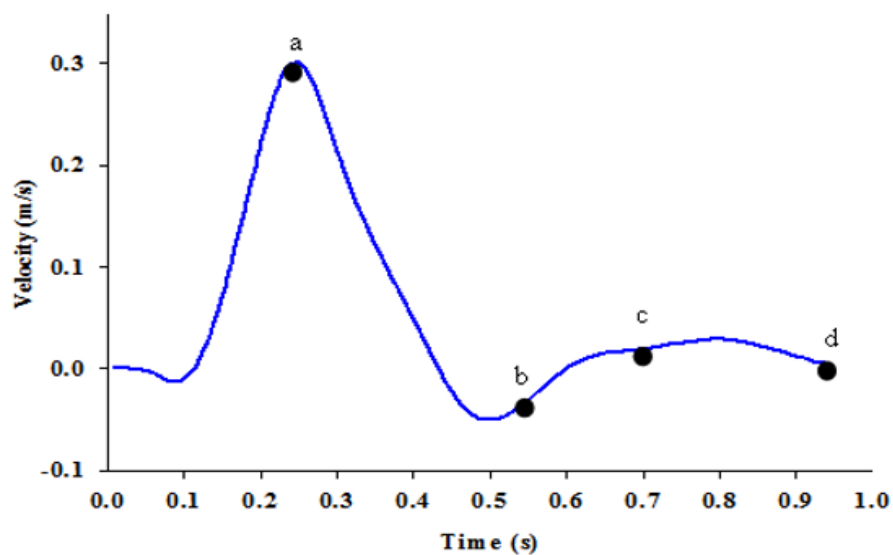
Figure 7: Velocity waveform imposed at the inlet.
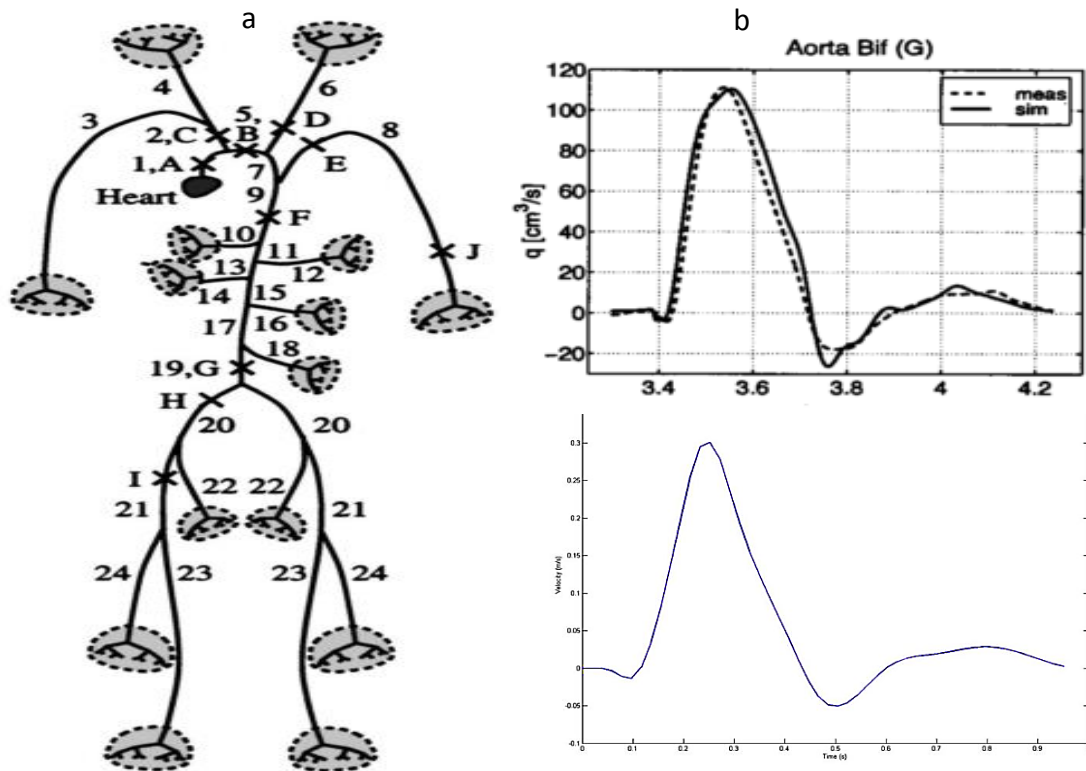
Figure 8: a: Areas of measured velocity, b: Velocity waveforms at G area (42,43).

3.4 Reynolds number

Reynolds number (Re) is defined as a unitless quantity that can determine whether the flow is turbulent or laminar. If Re is below 2000, the flow is laminar, however if it is more than 3000, the flow is turbulent. For Re between 2000 and 3000, it is considered unstable and tend to be either laminar or turbulent (45). Reynold number can be expressed as follows:

$$\text{Re} = \frac{\rho \vec{u} d}{\mu}$$

where μ and ρ are the viscosity and density of the fluid, $\vec{u}$ is the velocity and d is inlet diameter (46).

3.5 Governing equations

The laminar models were solved numerically based on Navier-Stokes equations of the momentum conservation and mass conservation for 3D incompressible and Newtonian fluid as following.

$$\rho(\vec{u} \cdot \nabla)\vec{u} + \nabla p - \mu \nabla \vec{u} = 0$$

$$\nabla \cdot \vec{u} = 0$$

Where ρ, μ, $\vec{u}$, P and ∇ denote density, dynamic viscosity, velocity, pressure, and gradient, respectively (47).

The turbulent model was solved by implementing Shear-Stress Transport (SST) k-omega (k-ω) model. The SST k-ω model was first developed and adopted by Menter (48) to accurately formulate the k-ω model in near-wall areas. According to both Banks et al.(49) and Ryval et al.(50) who found that this model was preferred for CFD turbulent flow simulations in arteries due to its better performances from other turbulence models when comparing the simulation outcomes against the results of experimental data.

3.6 Material properties

Blood through the aortas was assumed to be a homogenous. incompressible, and Newtonian fluid (51,52). These assumptions were acceptable in larger arteries with a constant dynamic viscosity and density of 0.0035 Pa.S and 1060 kg/m^3, respectively (24,51,53–55). The viscosity was approximately at a value of 45% of hematocrit (52). Furthermore, based on Reynolds number of 1696 in the 3D constructed models, the model was assumed to be laminar flow, while in the case of patient-specific geometry and the turbulent model was employed with Reynolds number of 2650.

3.7 Numerical simulation setup

For all simulations, the pressure-velocity coupling was set as SIMPLE algorithm to solve the continuity equation under 2nd order upwind momentum for

spatial discretization. The convergence criteria for the normalized continuity and velocity residuals were 1×10^{-5}. The CFD simulation of geometries was solved using finite volume solver, adopted by ANSYS Workbench v16.2 (ANSYS Inc., USA). However, for the transient study, A fixed time step of 0.01s was used and three cardiac cycles ($3 \times 0.94s$) =2.82s or 282 time-steps were completed for each simulation. All simulations were performed on a computer with a 16.0 GB RAM and 3.40 GHz quad-core processor.

4. Results and discussion

4.1 3D Constructed Geometry

Four angulated neck of AAA geometries with same aneurysm size of 5.5 cm in diameter and different angles were used to perform a steady state CFD simulation.

4.1.1 Flow patterns

The flow patterns through the angulated neck of AAA are presented in a longitudinal cross-section YZ-plane as illustrated in Figure 9. The thinning fluffy bar color of maximum velocity flow within the contours starts below renal arteries and continues cross the sac of aneurysm towards the bifurcation of aorta and ends up in outlet iliac arteries represented the impact of angulation on the blood flow behavior. This flow behaviors at the same time forms a thin bar line of maximum velocity which progressively increases in four different angulations due to change of angulated neck degree in AAA.

The visualization of streamlines for velocity is illustrated in Figure 10. Various recirculation vortexes were noticed within the aneurysm sac over the four angulated necks of aortas. But, when the angulated necks of abdominal aortic aneurysm increase, the vortex patterns within aneurysm become weakened and the velocity flow fields appear to be more concentrated in the center of aorta.
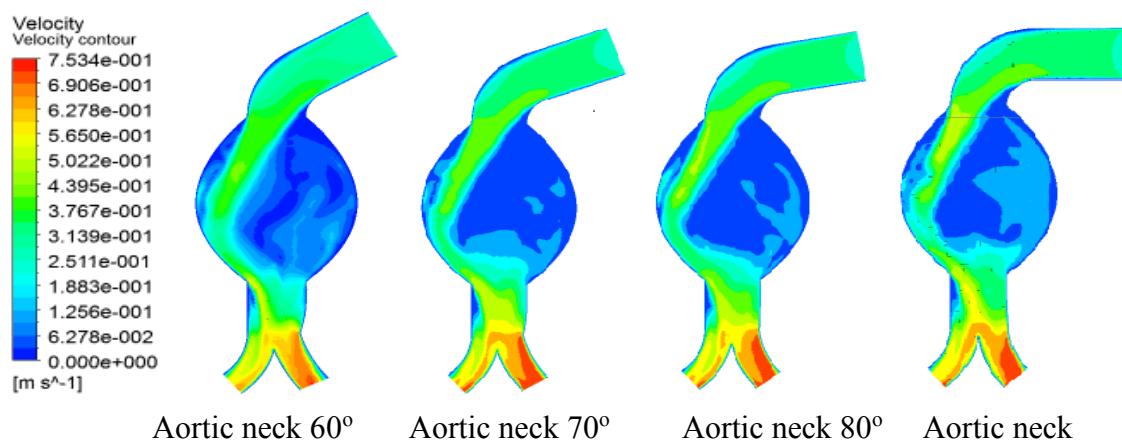

Figure 9: Velocity contours at the YZ-plane for the angulated neck of AAA.

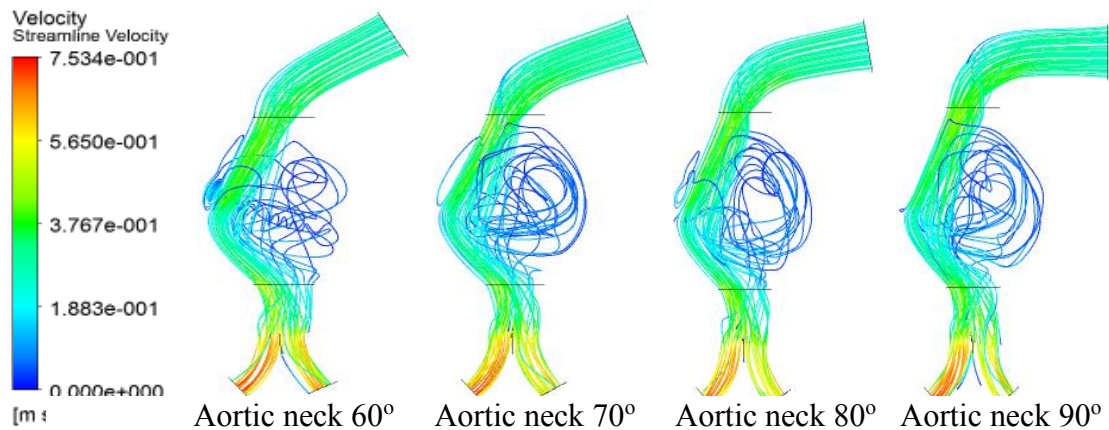Aortic neck 60º   Aortic neck 70º   Aortic neck 80º   Aortic neck 90º

Figure 10: Velocity streamlines of angulated neck of AAA.

For the flow behaviors at the proximal neck angulations are studied at the region of aortic bending which generates a particular angle between renal arteries and the onset of aneurysm formation. These flow behaviors are captured in detail at the four different aortic angles. The velocity contours of proximal neck of aortic aneurysm at the horizontal cross-sectional ZX-plane are shown in Figure 11a. The volume of blood flow was forming uncomplete circular form of velocity with lower velocity in angulated neck of 60º and 70º. The velocity through the angulated neck was measured on the cross-sectional plane of proximal neck using a horizontal line between the inner and outer walls (black point denotes inner wall and red for outer wall; see Figure 11a). Therefore, it is detected that when the angulated neck degrees increase, the velocity steadily also rises in the central region of proximal angulated neck as presented by chart in Figure 11b which displays the increment of lined-average velocity for four angulated neck of AAA models.

Furthermore, the contours presented in Figure 12 show the velocity flow pattern in aneurysm neck and how it differs in the four models. In order to predict the precise change of velocity flow fields at the neck, the reference points were given at proximal aneurysm sac as revealed in Figure 12a for this purpose. The 11-Points on the X-axis, point 0 represents inner wall and point 11 represents outer wall of the angulated neck of AAA. The velocity values obtained from the 11 points within the angulated neck of AAA are plotted in Figure 12b from point 0 to 12. It is clearly demonstrated that the

velocity rose gradually and the trend was upward until it reached maximum value of about 0.4 m/s at points 4 and 5; and then kept steadily in the same level in the central region of aortic neck with little fluctuation increasing in 80º and 90º angles and then it was slightly decreased at point 10 before it dropped sharply at point 11 to finally leveled off at the value zero at the outer wall of the distal neck. Even though, this simulation was performed with idealized fusiform models, but the simulation was based on realistic patient's information (56). As findings in our study, the numerical simulations of the four geometries of highly angulated neck of AAA using computational fluid dynamics (CFD) have confirmed that there is a significant influence on the velocity flow field due to the different degree of angular necks and their impacts on the flow downstream (23).
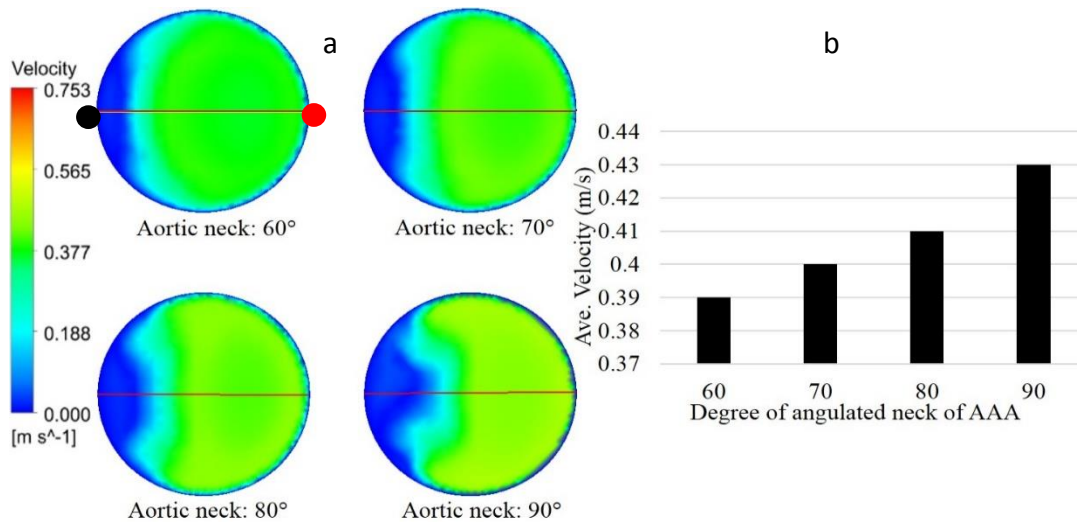

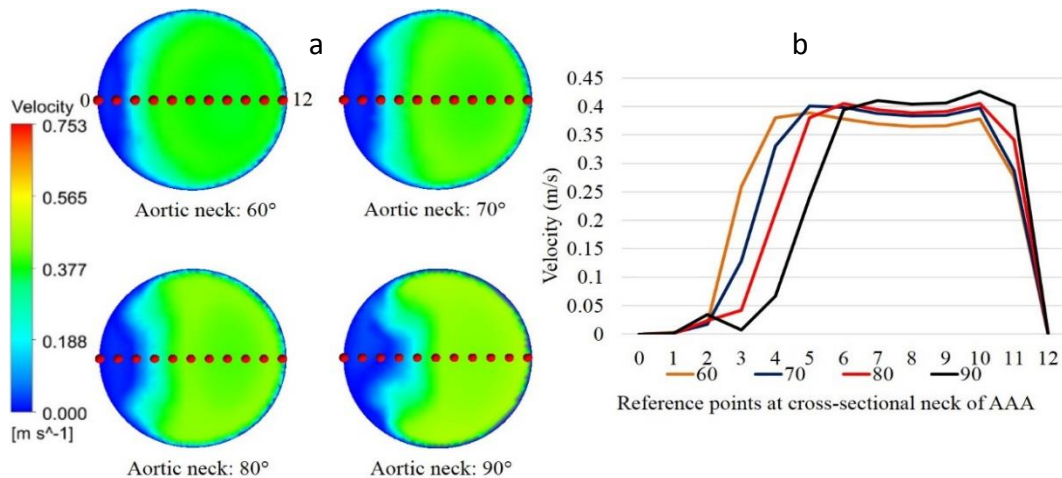Figure 11: a: Velocity at proximal neck of aneurysm, b: lined-average velocity.

Figure 12: a: Reference points at neck of AAA, b: Velocity at each point.

4.1.2 WSS distribution

The contours in Figure 13, are presented to clarify the wall shear stress (WSS) distribution on aortic wall surfaces for the four AAA models. As explained in flow pattern section, the velocity behavior influences the distribution of WSS which creates high WSS regions cross the models.

4.1.3 Pressure distribution

The calculation of pressure of idealized AAA models is illustrated in Figure 14. The contours show the distribution of pressure on the aortic wall and the aneurysm sac. In the four models, it is observed the pressure at the angular neck and at the distal end of the aneurysm regions are gradually increased, as the angles degree increases which results in maximum pressure in the model with 90°.

Aortic neck 60°   Aortic neck 70°   Aortic neck 80°   Aortic neck 90°
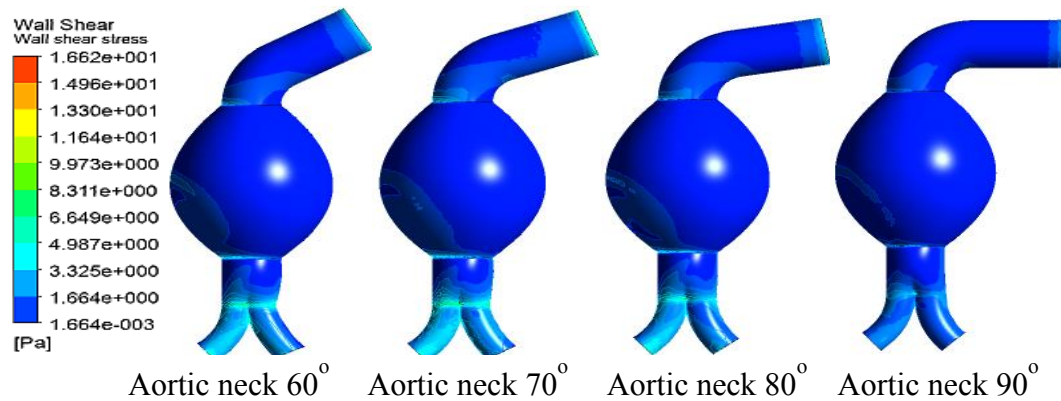
Figure 13: Distribution of WSS on the angulated neck of AAA models.

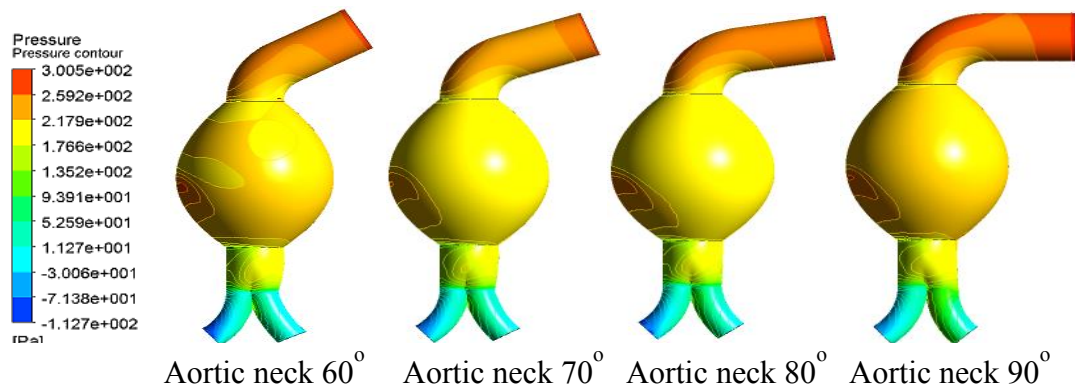Aortic neck 60°   Aortic neck 70°   Aortic neck 80°   Aortic neck 90°

Figure 14: Pressure distribution n wall of angulated neck of AAA models.

4.2 Patient-specific Geometry

The results of flow patterns and WSS in the transient condition are presented at four different time points of a cardiac cycle indicated by the points in Figure 7. These times are (a) peak systole t = 0.25 s, (b) early diastole t = 0.55 s, (c) mid-diastole t = 0.70 s, and (d) late diastole t = 0.94 s.

4.2.1   Flow patterns

The flow patterns are presented by the velocity contours in both horizontal and longitudinal cross-sections areas for the regions of interests (ROI) as shown in Figure 15a. The horizontal cross-sectional areas are indicated by planes (1 and 2) while plane (3) represents the vertical areas which extended from upper neck region towards the distal area of the sac as stated by the box. The contours of velocity within the horizontal cross-sectional slides in Figure 15b show that the magnitude of velocity is significantly changed over the time. The maximum velocity at the peak systole clearly seems to be higher by approximately 55% than other maximum velocities over the different time points in a cardiac cycle, while velocity flow among the diastolic stages show similarity with difference of only 4%. The flows within plane 2 tends to form a circular shape within the aortic that can cause a high blood recirculation while maintaining a low velocity at approximately 0.04 m/s. In the region of longitudinal cross-section, plane 3 emphasizes on the velocity flow starting from upper the neck bending region towards the distal sac of aneurysm for the ROI.

The contour at peak systole 0.25 s shows an arch shape of thin line of velocity flow entering the proximal angulated neck of aneurysm toward the sac and forming a bulk of blood flow near the outer wall of aorta, while it diminishes gradually over variant times through diastolic flow. At a full cardiac cycle 0.94 s, the flow in the aneurysm sac generates an interesting form of flow which can be clearly seen at the inner and outer sides of the artery wall. The graph in Figure 16; compares the maximum velocity for the three planes (1, 2 and 3) for the four different time-points of one cardiac cycle.

The streamlines of velocity flow are presented in Figure 17. The swirling of instantaneous velocity streamlines was acquired at different time points of a cardiac cycle. Distinguished lines of flows are displayed for ROI around the angular neck AAA. The recirculation blood vortexes are easily recognizable in various patterns over time.

Therefore, the impact of proximal angular neck on the flow within aneurysm sac was clearly showed to form a complex recirculation and flow impingement. This impact demonstrated a clear difference between the flow in AAA with proximal neck and without proximal neck as reported in previous study for AAA (57).
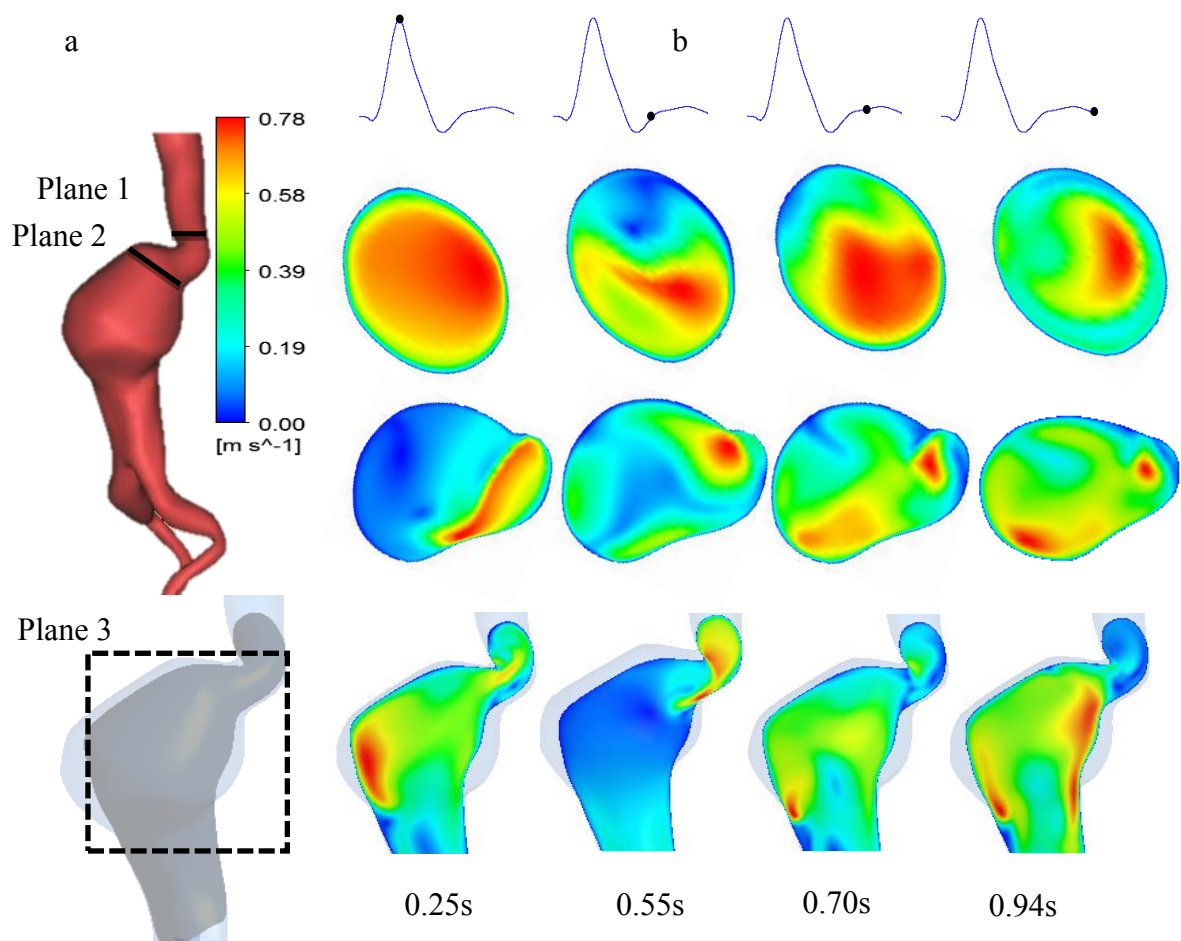

Figure 15: a: Selected areas indicated by planes, b: velocity at the four-time point.
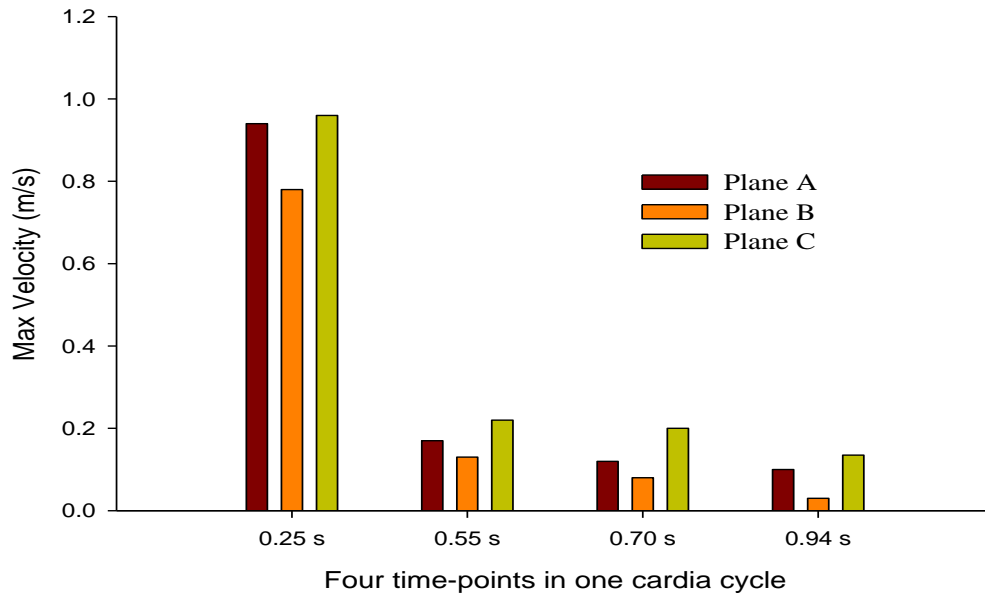
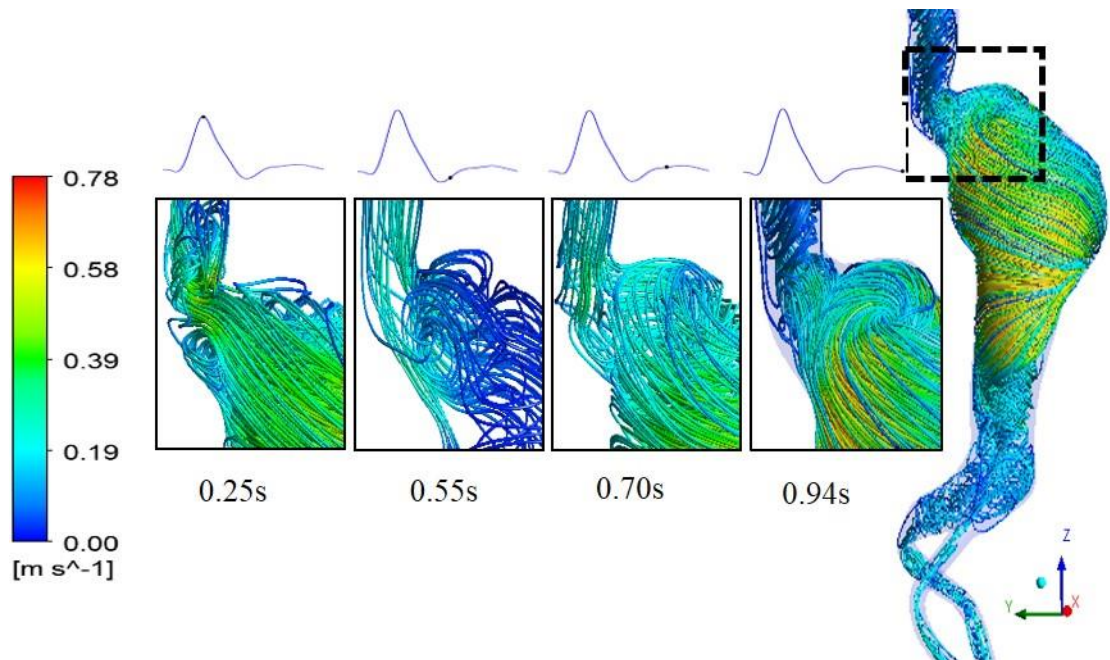Figure 16: Maximum velocity at four time-points of a cardiac cycle.

Figure 17: Streamline contours at four different time points in a cardiac cycle.

There are several factors that influence the hemodynamic, aortic rupture and the biomechanical conditions of arteries in cardiovascular disease (CVD). For instance, vascular geometry (58), elasticity of the wall (59), blood viscosity and pathological conditions. Furthermore, a larger diameter for ruptured AAAs was associated with greater recirculation flow whereas less recirculation was found in smaller ruptured AAAs (60). Therefore, this study reveals more complex recirculation and vorticity due to highly angulated neck and complexity of patient specific AAA geometry.

4.2.2 WSS distribution

The WSS distribution of four different time points of a cardiac cycle configuration (peak systole, early diastole, mid diastole and late diastole) for highly proximal neck angulation of AAA is depicted in Figure 18. The WSS distributions are illustrated in three different views. View 1 and 2 show the WSS in the inner and outer sides of the neck region, while view 3 illustrates the WSS distribution on the surface of aneurysm sac. We can observe that the high WSS of 1.24 Pa occurs at the area of proximal neck due to the turbulent flow exhibited within the region of angulation. The high bending, the severe tortuosity of aortic surface and asymmetric blood flow seem to be possible indicators of WSS and aortic rupture.

Our findings stated that a larger neck angle showed WSS can be located more diffuse across areas such as below the proximal neck, middle of sac as well as at the lower side of the aneurysm sac wall. It has been reported that high WSS can promote endothelial injury (61) while low WSS can lead to inflammatory infiltration (62). Therefore, this study has predicted a link between the behavior of blood flow and the change of WSS distribution. This correlation is consistent, and demonstrates an agreement with a previous study conducted by Arzani and Shadden (63).
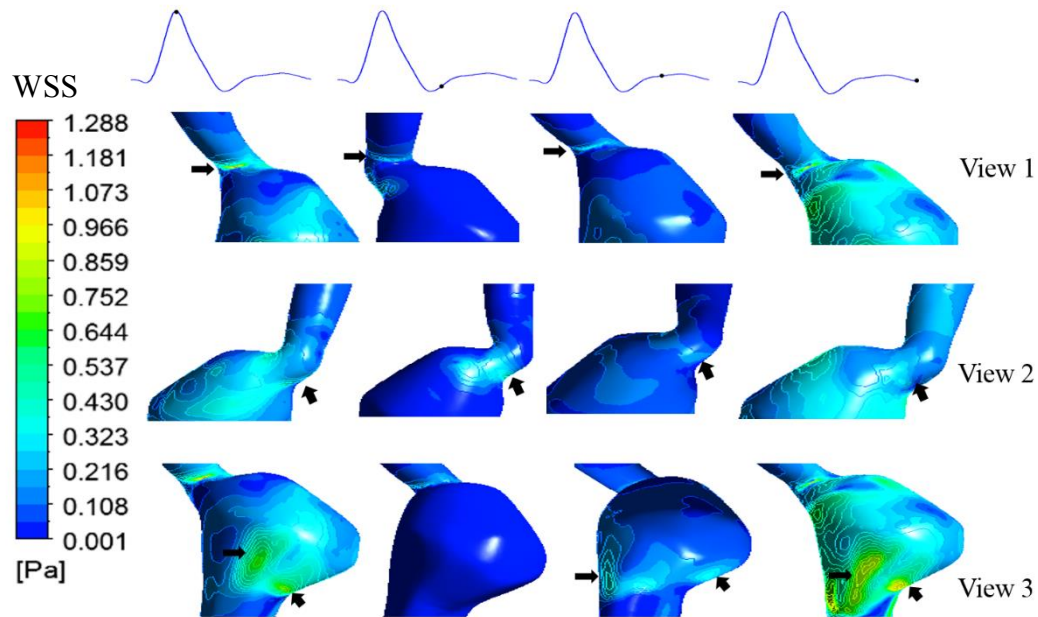
Figure 18:WSS distribution at four-time points in a cardiac cycle.

4.3 Limitations of study

The limitations of this work are divided for both cases. First, the limitations of 3D constructed simulations are that the designed AAA models are not representing the real domain of blood flow and the simulations were performed based on steady-state condition which do not comply with the nature of blood flow. Second, the patient-specific simulation may have some limitations since only one angulated neck of AAA patient-specific geometry was carried out for this simulation. However, it demonstrates the effect of geometrical features based on realistic time-varying velocity waveform, which is can be considered for personalized healthcare. It Is appropriate also to mention that this study implemented outflow boundary conditions at outlets which used the same waveform at the inlet of AAA section. This assumption is not expected to alter the overall findings as regards AAA neck angle and altered hemodynamics. Furthermore, it is worthy to point out that thrombus was not included in this study. The presence of intraluminal thrombus (ILT) encourages the change of geometrical features that can consequently influence the biomechanics of AAA (64). However, ILT was not involved in a scope of our study.

5. Conclusions

To sum up the concluding remarks of this study. Computational fluid dynamics techniques have proven to be a good tool to investigate the hemodynamic parameters such as flow patterns velocity field, blood pressure and as well as wall shear stress distribution on the aortic wall and aneurysm sac of angulated neck of idealized and real AAA geometries.

5.1 Idealized AAA models

The simulations were carried out with a steady-state flow condition. As the results showed, it is possible to predict the blood behaviors flowing in the proximal angular neck and aneurysm of three-dimensional angulated neck of AAA models. The WSS distribution was presented and the contours showed how blood flow behavior influences the distribution of WSS, which creates regions with high WSS. It is also observed that the pressure at the angular neck and at the distal end of the aneurysm regions are gradually increased, as the angles degree increase. Therefore, the numerical simulation has confirmed that there is an influence on the hemodynamic change because of the change of angular neck degrees.

5.2 Patient-specific geometry

The simulation in this case was done by performing transient fluid flow conditions to represent the nature of blood flow. The simulation concluded that the tortuosity of the aortic neck angulation causes a downstream of blood flow to be a turbulent flow and leads a weakening of the aortic wall, resulting in forming locations of high WSS. Thus, this study presented a comprehensive idea on the blood behavior in highly angulated necks of AAA and its influence on wall shear stress.

Thus, this study has shown that using computational fluid dynamics in pathological condition with a patient specific geometry can offer better visualizations for the flow of blood in cardiovascular system which is valuable for the interventional decisions regarding cardiovascular diseases.

6. Suggestions for future work

This study creates and presents a foundation and platform for understanding the computational modelling towards the blood flow behaviours within the angulated neck of AAA. Nevertheless, the following future suggestions are presented:

1. Additional patient-specific geometries for angulated neck of AAA are necessary to provide conclusive results and required parameters for more understanding the flow patterns within the region of interests.
2. Including the investigation of other hemodynamic parameters e.g. oscillatory shear index (OSI), time-averaged wall shear stress (TAWSS), relative residence time (RRT), and so on.
3. Considering applying more realistic boundary conditions e.g. time-dependent pressure and elastic aortic wall that comply with physiologic conditions.
4. Studying and simulating the blood arteries before and after the stent deployments to understand the effect of intervention on the blood flow behaviours and other hemodynamic parameters.

References

1. Waite L, Fine J. Applied Biofluid Mechanics. McGraw-Hill. 2007. 314p.

2. Sakalihasan N, Limet R, Defawe O. Abdominal aortic aneurysm. Lancet. 2005;365(9470):1577–89.

3. Humphrey JD, Taylor CA. Intracranial and abdominal aortic aneurysms: similarities, differences, and need for a new class of computational models. Annu Rev Biomed Eng. 2008;10:221–46.

4. Lozowy RJ, Kuhn DCSS, Ducas AA, Boyd AJ. The Relationship Between Pulsatile Flow Impingement and Intraluminal Thrombus Deposition in Abdominal Aortic Aneurysms. Cardiovasc Eng Technol. 2017 Mar;8(1):57–69.

5. Drewe CJ, Parker LP, Kelsey LJ, Norman PE, Powell JT, Doyle BJ. Haemodynamics and stresses in abdominal aortic aneurysms: A fluid-structure interaction study into the effect of proximal neck and iliac bifurcation angle. J Biomech. 2017;60:150–6.

6. Paramasivam V. A Conceptual Framework of a Novel Hybrid Methodology Between Computational Fluid Dynamics and Data Mining Techniques for Medical Dataset Application. Curtin University; 2017.

7. Kruchten T Van. CFD Modeling of Abdominal Aortic Aneurysms. Delft University of Technology; 2015.

8. Arzani A, Suh G-Y, Dalman RL, Shadden SC. A longitudinal comparison of hemodynamics and intraluminal thrombus deposition in abdominal aortic aneurysms. Am J Physiol Circ Physiol. 2014;307(12):H1786–95.

9. Ailawadi G, Eliason JL, Upchurch GR. Current concepts in the pathogenesis of abdominal aortic aneurysm. J Vasc Surg. 2003 Sep 1;38(3):584–8.

10. Blanchard JF. Epidemiology of abdominal aortic aneurysms. Epidemiol Rev. 1999;21(2):207–21.

11. Van Damme H, Sakalihasan N, Limet R. Factors promoting rupture of abdominal aortic aneurysms. Acta Chir Belg. 2005 Feb;105(1):1–11.

12. Wolf YG, Thomas WS, Brennan FJ, Goff WG, Sise MJ, Bernstein EF. Computed tomography scanning findings associated with rapid expansion of abdominal aortic aneurysms. J Vasc Surg. 1994 Oct 1;20(4):529–38.

13. Myers K, Devine T, Barras C, Self G. Endoluminal Versus Open Repair for Abdominal Aortic Aneurysms [Internet]. 2nd Virtual Congress of Cardiology. 2011 [cited 2017 Dec 12]. p. 1–37. Available from: http://www.fac.org.ar/scvc/llave/interven/myers/myersi.htm

14. Kleinstreuer C, Li Z. Analysis and computer program for rupture-risk prediction of abdominal aortic aneurysms. Biomed Eng Online. 2006 Mar 10;5(1):5–19.

15. Grootenboer N, Bosch JL, Hendriks JM, van Sambeek MRHM. Epidemiology, Aetiology, Risk of Rupture and Treatment of Abdominal Aortic Aneurysms: Does Sex Matter? Eur J Vasc Endovasc Surg. 2009 Sep 1;38(3):278–84.

16. Singh K, Bonaa KH, Jacobsen BK, Bjork L, Solberg S. Prevalence of and risk factors for abdominal aortic aneurysms in a population-based study : The Tromso Study. Am J Epidemiol. 2001 Aug 1;154(3):236–44.

17. O'Rourke MF, Hashimoto J. Mechanical Factors in Arterial Aging. A Clinical Perspective. J Am Coll Cardiol. 2007 Jul 3;50(1):1–13.

18. Lakatta EG, Wang M, Najjar SS. Arterial Aging and Subclinical Arterial Disease are Fundamentally Intertwined at Macroscopic and Molecular Levels. Vol. 93, Medical Clinics of North America. Elsevier; 2009. p. 583–604.

19. Enevoldsen MS, Henneberg KA, Jensen JA, Lönn L, Humphrey JD. New interpretation of arterial stiffening due to cigarette smoking using a structurally motivated constitutive model. J Biomech. 2011 Apr 7;44(6):1209–11.

20. Doll R. Mortality in relation to smoking: 50 years' observations on male British doctors. BMJ. 2004;328(7455):1519–0.

21. Kazi M, Thyberg J, Religa P, Roy J, Eriksson P, Hedin U, et al. Influence of intraluminal thrombus on structural and cellular composition of abdominal aortic aneurysm wall. J Vasc Surg. 2003 Dec 1;38(6):1283–92.

22. Sternbergh WC, Carter G, York JW, Yoselevitz M, Money SR. Aortic neck angulation predicts adverse outcome with endovascular abdominal aortic aneurysm repair. J Vasc Surg. 2002;35(3):482–6.

23. Yeow SL, Leo HL. Hemodynamic Study of Flow Remodeling Stent Graft for the Treatment of Highly Angulated Abdominal Aortic Aneurysm. Comput Math Methods Med. 2016 May 9;2016:1–10.

24. Xenos M, Alemu Y, Zamfir D, Einav S, Ricotta JJ, Labropoulos N, et al. The effect of angulation in abdominal aortic aneurysms: Fluid-structure interaction simulations of idealized geometries. Med Biol Eng Comput. 2010 Dec 19;48(12):1175–90.

25. Morrison TM, Meyer CA, Fillinger MF, Fairman RM, Glickman MH, Cambria RP, et al. Eligiblity for Endovascular Repair of Short Neck Abdominal Aortic Aneurysms. J Vasc Surg. 2013;57(5):24S.

26. Raghavan ML, Vorp DA, Federle MP, Makaroun MS, Webster MW. Wall stress distribution on three-dimensionally reconstructed models of human abdominal aortic aneurysm. J Vasc Surg. 2000;31(4):760–9.

27. del Álamo JC, Marsden AL, Lasherasa JC. Recent Advances in the Application of Computational Mechanics to the Diagnosis and Treatment of Cardiovascular Disease. Rev Española Cardiol (English Ed. 2009 Jun 1;62(7):781–805.

28. Fillinger MF, Marra SP, Raghavan ML, Kennedy FE. Prediction of rupture risk in abdominal aortic aneurysm during observation: Wall stress versus diameter. J Vasc Surg. 2003 Apr 1;37(4):724–32.

29. Di Martino ES, Vorp DA. Effect of variation in intraluminal thrombus constitutive properties on abdominal aortic aneurysm wall stress. Ann Biomed

Eng. 2003 Jul;31(7):804–9.

30. Raghavan ML, Fillinger MF, Marra SP, Naegelein BP, Kennedy FE. Automated Methodology for Determination of Stress Distribution in Human Abdominal Aortic Aneurysm. J Biomech Eng. 2005 Oct 1;127(5):868–71.

31. Di Martino ES, Guadagni G, Fumero A, Ballerini G, Spirito R, Biglioli P, et al. Fluid-structure interaction within realistic three-dimensional models of the aneurysmatic aorta as a guidance to assess the risk of rupture of the aneurysm. Med Eng Phys. 2001 Nov 1;23(9):647–55.

32. Li Z, Kleinstreuer C. A new wall stress equation for aneurysm-rupture prediction. Ann Biomed Eng. 2005 Feb;33(2):209–13.

33. Morris PD, Narracott A, Von Tengg-Kobligk H, Soto DAS, Hsiao S, Lungu A, et al. Computational fluid dynamics modelling in cardiovascular medicine. Heart. 2016;102(1):18–28.

34. Taylor CA, Figueroa CA. Patient-Specific Modeling of Cardiovascular Mechanics. Annu Rev Biomed Eng. 2009 Aug 10;11(1):109–34.

35. Glor FP, Long Q, Hughes AD, Augst AD, Ariff B, Mcg Thom SA, et al. Reproducibility study of magnetic resonance image-based computational fluid dynamics prediction of carotid bifurcation flow. Ann Biomed Eng. 2003 Feb;31(2):142–51.

36. Chung B, Cebral JR. CFD for Evaluation and Treatment Planning of Aneurysms: Review of Proposed Clinical Uses and Their Challenges. Ann Biomed Eng. 2014;43(1):122–38.

37. Li Z, Kleinstreuer C. Analysis of biomechanical factors affecting stent-graft migration in an abdominal aortic aneurysm model. J Biomech. 2006 Jan 1;39(12):2264–73.

38. Tong J, Schriefl a. JJ, Cohnert T, Holzapfel G a. A. Gender Differences in Biomechanical Properties, Thrombus Age, Mass Fraction and Clinical Factors

of Abdominal Aortic Aneurysms. Eur J Vasc Endovasc Surg. 2013;45(4):364–72.

39.   Georgakarakos E, Ioannou C V., Kamarianakis Y, Papaharilaou Y, Kostas T, Manousaki E, et al. The Role of Geometric Parameters in the Prediction of Abdominal Aortic Aneurysm Wall Stress. Eur J Vasc Endovasc Surg. 2010;39(1):42–8.

40.   Taylor TW, Yamaguchi T. Three-dimensional simulation of blood flow in an abdominal aortic aneurysm - Steady and unsteady flow cases. J Biomech Eng. 1994;116(1):89–97.

41.   ChungDann Kan TC. Numerical Simulation of Blood Flow in Double-Barreled Cannon EVAR and its Clinical Validation. J Vasc Med Surg. 2014 Oct 20;2(4).

42.   Rissland P, Alemu Y, Einav S, Ricotta J, Bluestein D. Abdominal Aortic Aneurysm Risk of Rupture: Patient-Specific FSI Simulations Using Anisotropic Model. J Biomech Eng. 2009 Mar 1;131(3):31001.

43.   Olufsen MS, Peskin CS, Kim WY, Pedersen EM, Nadim A, Larsen J. Numerical simulation and experimental validation of blood flow in arteries with structured-tree outflow conditions. Ann Biomed Eng. 2000;28(11):1281–99.

44.   Morbiducci U, Gallo D, Massai D, Consolo F, Ponzini R, Antiga L, et al. Outflow conditions for image-based hemodynamic models of the carotid bifurcation: implications for indicators of abnormal flow. J Bomechanical Eng. 2010;132(9):91005.

45.   OpenStax College. College Physics. Vol. 12, Physics Today. 1959. 62-64 p.

46.   Molony DS, Callanan A, Morris LG, Doyle BJ, Walsh MT, McGloughlin TM. Geometrical enhancements for abdominal aortic stent-grafts. J Endovasc Ther. 2008;15(5):518–29.

47.   Zhang P, Sun A, Zhan F, Luan J, Deng X. Hemodynamic study of overlapping bare-metal stents intervention to aortic aneurysm. J Biomech.

2014;47(14):3524–30.

48.   Menter FR, Kuntz M, Langtry R. Ten Years of Industrial Experience with the SST Turbulence Model. Turbul Heat Mass Transf 4. 2003;4:625–32.

49.   Banks J, Bressloff NW. Turbulence Modeling in Three-Dimensional Stenosed Arterial Bifurcations. J Biomech Eng. 2007;129(1):40–50.

50.   Ryval J, Straatman AG, Steinman DA. Two-equation Turbulence Modeling of Pulsatile Flow in a Stenosed Tube. J Biomech Eng. 2004;126(5):625–35.

51.   Algabri YA, Rookkapan S, Chatpun S. Three-dimensional finite volume modelling of blood flow in simulated angular neck abdominal aortic aneurysm. IOP Conf Ser Mater Sci Eng. 2017 Sep;243(1):12003.

52.   Carty G, Chatpun S, Espino DM. Modeling Blood Flow Through Intracranial Aneurysms: A Comparison of Newtonian and Non-Newtonian Viscosity. J Med Biol Eng. 2016;36(3):396–409.

53.   Morris L, Delassus P, Callanan A, Walsh M, Wallis F, Grace P, et al. 3-D Numerical Simulation of Blood Flow Through Models of the Human Aorta. J Biomech Eng. 2005;127(5):767–75.

54.   Renner J, Loyd D, Länne T, Karlsson M. Is a flat inlet profile sufficient for WSS estimation in the aortic arch? WSEAS Trans Fluid Mech. 2009;4(4):148–60.

55.   Owen B, Lowe C, Ashton N, Mandal P, Rogers S, Wein W, et al. Computational hemodynamics of abdominal aortic aneurysms: Three-dimensional ultrasound versus computed tomography. Proc Inst Mech Eng Part H J Eng Med. 2016;230(3):201–10.

56.   Li Z, Kleinstreuer C. A comparison between different asymmetric abdominal aortic aneurysm morphologies employing computational fluid-structure interaction analysis. Eur J Mech B/Fluids. 2007;26(5):615–31.

57.   Finol EA, Keyhani K, Amon CH. The Effect of Asymmetry in Abdominal Aortic

Aneurysms Under Physiologically Realistic Pulsatile Flow Conditions. J Biomech Eng. 2003 Apr 1;125(2):207–17.

58. Gounley J, Vardhan M, Randles A. A Computational Framework to Assess the Influence of Changes in Vascular Geometry on Blood Flow. In: Proceedings of the Platform for Advanced Scientific Computing Conference on - PASC '17. Lugano; 2017. p. 1–8.

59. Bokov P, Flaud P, Bensalah A, Fullana J-M, Rossi M. Implementing Boundary Conditions in Simulations of Arterial Flows. J Biomech Eng. 2013 Sep 24;135(11):111004.

60. Boyd AJ, Kuhn DCS, Lozowy RJ, Kulbisky GP. Low wall shear stress predominates at sites of abdominal aortic aneurysm rupture. J Vasc Surg. 2016;63(6):1613–9.

61. Langille BL, O'Donnell F. Reductions in arterial diameter produced by chronic decreases in blood flow are endothelium-dependent. Science (80-). 1986 Jan 24;231(4736):405–7.

62. Zarins CK, Giddens DP, Bharadvaj BK, Sottiurai VS, Mabon RF, Glagov S. Carotid bifurcation atherosclerosis. Quantitative correlation of plaque localization with flow velocity profiles and wall shear stress. Circ Res. 1983 Oct 1;53(4):502–14.

63. Arzani A, Shadden SC. Characterizations and Correlations of Wall Shear Stress in Aneurysmal Flow. J Biomech Eng. 2015;138(1):14503.

64. Deplano V, Knapp Y, Bailly L, Bertrand E. Flow of a blood analogue fluid in a compliant abdominal aortic aneurysm model: Experimental modelling. J Biomech. 2014 Apr;47(6):1262–9.

65. Chen D, Müller-Eschner M, Kotelis D, Böckler D, Ventikos Y, Von Tengg-Kobligk H. A longitudinal study of Type-B aortic dissection and endovascular repair scenarios: Computational analyses. Med Eng Phys. 2013 Sep

1;35(9):1321–30.

66. Karmonik C, Duran C, Davies MG, Shah DJ, Lumsden AB, Bismuth J. Correlation between hemodynamic parameters and intra-arterial septum motion in DeBakey type III aortic dissections using 2D pcMRI and 4D MRA. In: Proceedings of the Annual International Conference of the IEEE Engineering in Medicine and Biology Society, EMBS. Boston, MA: IEEE; 2011. p. 2809–12.

67. Cheng Z, Tan FPP, Riga C V., Bicknell CD, Hamady MS, Gibbs RGJ, et al. Analysis of Flow Patterns in a Patient-Specific Aortic Dissection Model. J Biomech Eng. 2010 May 1;132(5):51007.

68. Tse KM, Chiu P, Lee HP, Ho P. Investigation of hemodynamics in the development of dissecting aneurysm within patient-specific dissecting aneurismal aortas using computational fluid dynamics (CFD) simulations. J Biomech. 2011 Mar 15;44(5):827–36.

69. Fung GSK, Lam SK, Cheng SWK, Chow KW. On stent-graft models in thoracic aortic endovascular repair: A computational investigation of the hemodynamic factors. Comput Biol Med. 2008 Apr 1;38(4):484–9.

70. Cheng SWK, Lam ESK, Fung GSK, Ho P, Ting ACW, Chow KW. A computational fluid dynamic study of stent graft remodeling after endovascular repair of thoracic aortic dissections. J Vasc Surg. 2008 Aug 1;48(2):303–10.

71. Lam SK, Fung GSK, Cheng SWK, Chow KW. A computational study on the biomechanical factors related to stent-graft models in the thoracic aorta. Med Biol Eng Comput. 2008 Nov 11;46(11):1129–38.

72. Karmonik C, Bismuth J, Redel T, Anaya-Ayala JE, Davies MG, Shah DJ, et al. Impact of tear location on hemodynamics in a type B aortic dissection investigated with computational fluid dynamics. In: 2010 Annual International Conference of the IEEE Engineering in Medicine and Biology Society, EMBC'10. IEEE; 2010. p. 3138–41.

73. Karmonik C, Bismuth J, Shah DJ, Davies MG, Purdy D, Lumsden AB. Computational study of haemodynamic effects of entry- and exit-tear coverage in a DeBakey type III aortic dissection: Technical report. Eur J Vasc Endovasc Surg. 2011 Aug 1;42(2):172–7.

74. Karmonik C, Bismuth J, Davies MG, Shah DJ, Younes HK, Lumsden AB. A Computational Fluid Dynamics Study Pre- and Post-Stent Graft Placement in an Acute Type B Aortic Dissection. Vasc Endovascular Surg. 2011 Feb 13;45(2):157–64.

75. Karmonik C, Partovi S, Müller-Eschner M, Bismuth J, Davies MG, Shah DJ, et al. Longitudinal computational fluid dynamics study of aneurysmal dilatation in a chronic DeBakey type III aortic dissection. J Vasc Surg. 2012 Jul 1;56(1):260–263.e1.

76. Midulla M, Moreno R, Baali A, Chau M, Negre-Salvayre A, Nicoud F, et al. Haemodynamic imaging of thoracic stent-grafts by computational fluid dynamics (CFD): Presentation of a patient-specific method combining magnetic resonance imaging and numerical simulations. Eur Radiol. 2012 Oct 30;22(10):2094–102.

77. WAN AB NAIM WN, GANESAN PB, SUN Z, OSMAN K, LIM E. THE IMPACT OF THE NUMBER OF TEARS IN PATIENT-SPECIFIC STANFORD TYPE B AORTIC DISSECTING ANEURYSM: CFD SIMULATION. J Mech Med Biol. 2014 Apr 10;14(2):1450017.

78. Fan Y, Cheng SW-K, Qing K-X, Chow K-W. Endovascular repair of type B aortic dissection: a study by computational fluid dynamics. J Biomed Sci Eng. 2010;3(9):900–7.

79. Tang AYS, Fan Y, Cheng SWK, Chow KW. Biomechanical Factors Influencing Type B Thoracic Aortic Dissection: Computational Fluid Dynamics Study. Eng Appl Comput Fluid Mech. 2012 Jan 19;6(4):622–32.

80. Rudenick PA, Bordone M, Bijnens BH, Soudah E, Oñate E, Garcia-Dorado D,

et al. A Multi-method Approach towards Understanding the Pathophysiology of Aortic Dissections – The Complementary Role of In-Silico, In-Vitro and In-Vivo Information. In Springer, Berlin, Heidelberg; 2010. p. 114–23.

81. Hou G, Tsagakis K, Wendt D, Jakob H, Kowalczyk W, Dynamics CF, et al. Three-phase numerical simulation of blood flow in the ascending aorta with dissection. V Eur Conf Comput Fluid Dyn ECCOMAS CFD 2010. 2010;(June):14–7.

82. Gao F, Watanabe M, Matsuzawa T. Stress analysis in a layered aortic arch model under pulsatile blood flow. Biomed Eng Online. 2006;5.

83. Khanafer K, Berguer R. Fluid-structure interaction analysis of turbulent pulsatile flow within a layered aortic wall as related to aortic dissection. J Biomech. 2009 Dec 11;42(16):2642–8.

Appendices

Appendix A

User-defined Function

```
/* UDFs for specifying time dependent velocity profile                          */
/*                                                                              */
/********************************************************************************/
//Written by Yousif
//PSU

#include "udf.h"

//inlet velocity waveform
DEFINE_PROFILE (inlet_velocity, thread, position)
{
face_t f;

double w;
double a0, a1, a2, a3, a4, a5, a6, a7, a8;
double    b1, b2, b3, b4, b5, b6, b7, b8;

            a0 =     0.05282  ;
            a1 =     -0.003823  ;
            b1 =     0.0855   ;
            a2 =     -0.07917  ;
            b2 =     -0.03871  ;
            a3 =     0.02291  ;
            b3 =     -0.03364  ;
            a4 =     0.01638  ;
            b4 =     0.000165 ;
            a5 =     0.00169  ;
            b5 =     0.01464  ;
            a6 =     -0.006033  ;
            b6 =     -0.0001296 ;
            a7 =     0.000763  ;
            b7 =     -0.001647  ;
            a8 =     0.0002712 ;
            b8 =     0.00152   ;
             w =      6.739    ;

begin_f_loop(f, thread)
double t = RP_Get_Real("flow-time"); //t is the local time within each period
      {
```

```
F_PROFILE(f, thread, position) = a0 + a1*cos(t*w) + b1*sin(t*w) + \
  a2*cos(2*t*w) + b2*sin(2*t*w) + a3*cos(3*t*w) + b3*sin(3*t*w) + \
  a4*cos(4*t*w) + b4*sin(4*t*w) + a5*cos(5*t*w) + b5*sin(5*t*w) + \
  a6*cos(6*t*w) + b6*sin(6*t*w) + a7*cos(7*t*w) + b7*sin(7*t*w) + \
  a8*cos(8*t*w) + b8*sin(8*t*w);

}
end_f_loop(f, thread)
}
```

Appendix B

Table E1: Summary of the numerical simulation settings for aortic.

No.	Imaging modalities	Geometrical parameters	No of models	Flow	Blood properties	Wall	Reference
Patient-specific (Realistic) geometries							
1	CT & MRA	—	2	Laminar	Newtonian	Rigid	Chen et al., 2013.(65)
2	CT	—	4	Transitional flow	Newtonian	Rigid	Karmonik et al., 2011.(66)
3	CT	Inlet diameter (ascending aorta) = 36.0mm	1	Transitional flow	Newtonian & non-Newtonian (Quemada model)	Rigid	Cheng et al., 2010.(67)
4	CT	—	2	Laminar	Newtonian	Rigid	Tse et al., 2011.(68)
5	CT	—	1	Laminar	Newtonian	Rigid	Fung et al., 2008.(69)
6	CT	—	12	Laminar	Newtonian	Rigid	Cheng et al., 2008.(70)
7	CT	—	1	Laminar	Newtonian	Rigid	Lam et al., 2008.(71)
8	MRI	—	1	Laminar	Newtonian	Rigid	Karmonik et al., 2010.(72)
9	MRI	—	1	Laminar	Newtonian	Rigid	Karmonik et al., 2011.(73)
10	MRI	—	1	Laminar	Newtonian	Rigid	Karmonik et al., 2011.(74)
11	MRI	—	1	Laminar	Newtonian	Rigid	Karmonik et al., 2012.(75)
12	MRA	—	6			Prescribed wall movement	Midulla et al., 2015.(76)
13	CT	—	1	Laminar	Newtonian	Fluid-Structure	Wan Naimah et

						Interaction (FSI)	al., 2013.(77)
14	CT	Inflow inlet diameter = 25.0mm	1	Turbulent: K-omega	Newtonian	Rigid	Algabri et al., 2018.

Ideal geometries

15	—	Inlet diameter (ascending aorta) = 30.0mm Curvature diameter of the aortic arch = 93.0mm	—	Laminar	Newtonian	Rigid	Fan et al., 2010.(78)
16	—	Inlet diameter (ascending aorta) = 30.0mm Curvature diameter of the aortic arch = 120.0mm	—	Turbulent k-epsilon	Newtonian	Rigid	Tang et al., 2012.(79)
17	—	Inlet diameter (ascending aorta) = 20.0mm Intimal flap thickness = 2mm	—	Laminar	Newtonian	Rigid	Rudenick et al., 2010.(80)
18	—	Inlet diameter (ascending aorta) = 25.0mm	—	Turbulent: SST K-W	Newtonian	Rigid	Hou et al., 2010.(81)
19	—	—	—	—	Newtonian	FSI	Gao et al., 2006.(82)
20	—	—	—	Turbulent: SST K-W	Newtonian	FSI	Khanafer et al., 2009.(83)
21	Solid Work	Inlet diameter =20.0mm		Laminae	Newtonian	Rigid	Algabri et al., 2017.(51)

Appendix C

Papers and Proceedings

Table E2: Review of papers/ proceedings and status

S/N	Title	Type	Status
1.	The impact of angular neck in abdominal aortic aneurysm: computational fluid dynamics simulations of patient specific geometry	Abstract: Conference	Accepted for Oral Presentation at 1st PSU-UNS Joint Conference on Medical Science and Technology 2018 (JCMST 2018), 5- 7 Mar 2018, krabi, Thailand
2.	Computational study on hemodynamic changes in patient-specific proximal neck angulation of abdominal aortic aneurysm with time-varying velocity	Research Paper	Submitted to Arabian Journal for Science and Engineering (Under review)
3.	Three-dimensional finite volume modelling of blood flow in simulated angular neck abdominal aortic aneurysm	Conference Proceeding	Accepted for Oral Presentation at the 2nd International Conference on Computational Fluid Dynamics in Research and Industry 3-4 Aug 2018, Songkla, Thailand
4.	Three-dimensional finite volume modelling of blood flow in simulated angular neck abdominal aortic aneurysm	Research Paper	Accepted and published in IOP Conference series Elsevier (index in Scopus)

THE IMPACT OF ANGULAR NECK IN ABDOMINAL AORTIC ANEURYSM: COMPUTATIONAL FLUID DYNAMICS SIMULATIONS OF PATIENT SPECIFIC GEOMETRY

Yousif Ali Algabri[1], Sorracha Rookaphan[2], Surapong Chatpun[1]

[1]Institute of Biomedical Engineering, Faculty of Medicine, Prince of Songkla University, HatYai, Songkhla, Thailand
algabriyousif80@gmail.com, surapong.c@psu.ac.th

[2]Department of Radiology, Faculty of Medicine, Prince of Songkla University, Hat Yai, Songkhla, Thailand
srookkapan@gmail.com

Introduction:
Abdominal aortic aneurysm (AAA) is globally considered one of the most popular cardiovascular pathologies. The aneurysm is categorized as a localized expansion of the diameter of abdominal aorta by at least 1.5 times the normal diameter. It is as well found to be the 13th leading reason of mortality rate in US. Apart from AAA diameter, there are other significant factors to be considered when assessing the rupture risks, such as asymmetry flow, proximal neck and bifurcation angle. Although proximal aortic neck is often measured in clinical practice, it has not got attention in relation to the biomechanics. We aimed to perform the finite volume method on a patient specific geometry to study the influence of proximal neck angle abdominal aortic aneurysm on the flow behaviors and AAA wall shear stress (WSS).

Materials and methods:
Computer tomography (CT) scan data was obtained in a DICOM file from a pre-operative AAA patient. The 3D smoothed geometry was reconstructed by using Mimics software. The aneurysm diameter was measured as 56 mm with angular neck of 79 degree. The tetrahedron method was applied for meshing the geometry in ICEM CFD. The mesh dependency study was performed for three different numbers of elements. They were coarse (519,166 elements), fine (753,780 elements), and finer (939,537 elements). The transient numerical simulations were carried out by using computational fluid dynamics (CFD) to solve governing equations in ANSYS Fluent v16.2. The boundary conditions were based on literature reviews for pulsating blood flow and the aortic wall was assumed to be rigid and no-slip. Blood was also assumed as Newtonian and incompressible fluid with the density and dynamic viscosity of 1,060 kg/m^3 and 0.0035 Pa·S, respectively.

Findings:

It was found that the finer mesh provided more accurate results. The results also indicate that the blood flow at the proximal aneurysm neck have higher velocity values which lead to the increase of WSS. The velocity contour presented in Figure 1a is at the peak systole, the contour showed maximum velocity was developed within the proximal neck and aneurysm sac into several circulation zones and vortices producing turbulent flow towards the bifurcation regions. The behaviors of flow and vortices generate high WSS at the regions as illustrated in Figure 1b. The position of peak WSS is located at the bottom of aneurysm because of asymmetrical flow that caused by the tortuosity of aortic neck. The flow rate and pressure were analyzed and correlated with potential change in WSS.
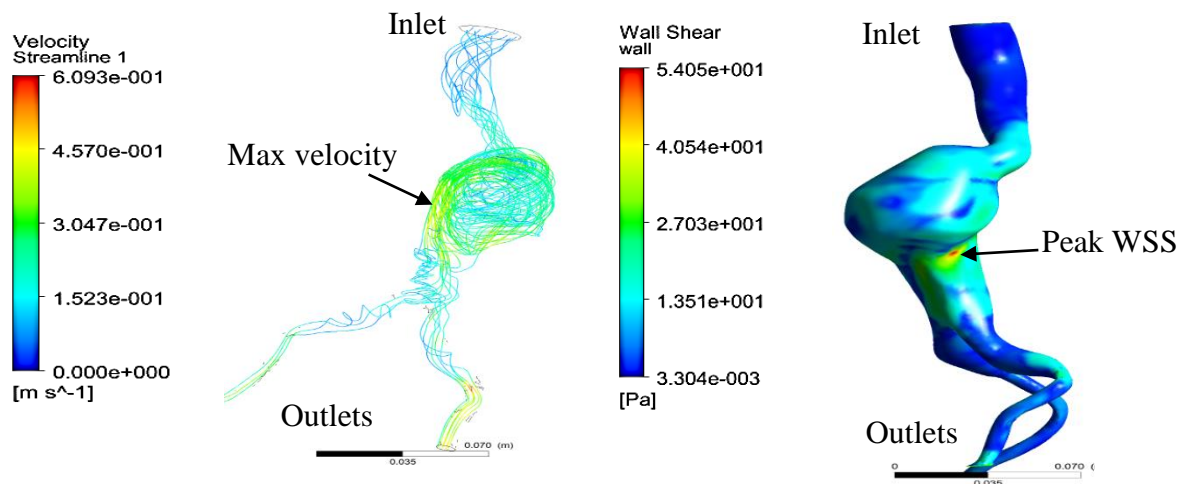
Figure 1 (a) Maximum velocity and (b) Peak wall shear stress (WSS) occurred in angular neck abdominal aortic aneurysm

Conclusion:

Eventually, the numerical approaches can be used to determine the change of hemodynamics in a complicated geometry of cardiovascular system using a patient specific model to provide a clear understanding for clinical practitioners and surgical procedures.

*Keywords***:** Abdominal aortic aneurysm, patient specific model, computational fluid dynamics, hemodynamics.

Arabian Journal for Science and Engineering
Computational study on hemodynamic changes in patient-specific proximal neck angulation of abdominal aortic aneurysm with time-varying velocity
--Manuscript Draft--

| Abstract: | Aneurysms are considered as a critical cardiovascular disease worldwide when they rupture. The clinical understanding of geometrical impact on the flow behaviour and biomechanics of abdominal aortic aneurysm (AAA) is progressively developing. Proximal neck angulations of AAAs are believed to influence the hemodynamic changes and wall shear stress (WSS) within AAAs. Our aim was to perform pulsatile simulations using computational fluid dynamics (CFD) for patient-specific geometry to investigate the influence of severe angular (≥ 60) neck on AAA's hemodynamic and wall shear stress. The patient's geometrical characteristics were obtained from a computed tomography images database of AAA patients. The AAA geometry was reconstructed using Mimics software. In computational method, blood was assumed Newtonian fluid and an inlet varying velocity waveform in a cardiac cycle was assigned. The CFD study was performed with ANSYS software. The results of flow behaviours indicated that the blood flow through severe bending of angular neck leads to high turbulence and asymmetry of flows within the aneurysm sac resulting in blood recirculation. The high wall shear stress (WSS) occurred near the AAA neck and on surface of aneurysm sac. This study explained and showed flow behaviours and WSS progression within high angular neck AAA and risk predication of abdominal aorta rupture. We expect that the visualization of blood flow and hemodynamic changes resulted from CFD simulation could be as an extra tool to assist clinicians during a |

	decision making when estimation the risks of interventional procedures.
Suggested Reviewers:	Kahar Osman, Ph.D. Associate Professor, Universiti Teknologi Malaysia kaharosman@utm.my His expertise is in Computational Fluid Dynamics (CFD) with many publications in CFD in medicine. He is an associate member at IJN-UTM Cardiovascular Engineering Centre.
	Woong Chol Kang, M.D. Gachon University Gil Medical Center kangwch@gilhospital.com He has work related to angulation of aortic neck endovascular repair.
	Hui Meng, Ph.D. University at Buffalo - The State University of New York huimeng@buffalo.edu He has published paper related to computational fluid dynamics and intracranial aneurysm.
	Raúl Antón, Ph.D. Universidad de Navarra ranton@tecnun.es His expertise is about computational fluid dynamics, hemodynamics. He also published paper about the patient-specific abdominal aortic anuerysm

Computational study on hemodynamic changes in patient-specific proximal neck angulation of abdominal aortic aneurysm with time-varying velocity

Yousif A. Algabri[1], Sorracha Rookkapan[2], Vera Gramina[3], Daniel M. Espino[4], and

Surapong Chatpun[1]

[1]Institute of Biomedical Engineering, Faculty of Medicine, Prince of Songkla University,

HatYai 90110, Thailand

[2]Department of Radiology, Faculty of Medicine, Prince of Songkla University, HatYai

90110, Thailand

3Neuroscience Research Center, University Magna Graecia, Catanzaro, 88100, Italy

[4]Department of Mechanical Engineering, University of Birmingham, Birmingham, B15 2TT,

UK

Correspondence to:

Surapong Chatpun, Ph.D.

Institute of Biomedical Engineering, Faculty of Medicine, Prince of Songkla University

6th floor, 100-year Building Hatyai, Songkhla, 90110 Thailand

e-mail: surapong.c@psu.ac.th

Conflict of interest

The authors reported that no conflict of interest in this research.

2

Abstract

Aneurysms are considered as a critical cardiovascular disease worldwide when they rupture. The clinical understanding of geometrical impact on the flow behaviour and biomechanics of abdominal aortic aneurysm (AAA) is progressively developing. Proximal neck angulations of AAAs are believed to influence the hemodynamic changes and wall shear stress (WSS) within AAAs. Our aim was to perform pulsatile simulations using computational fluid dynamics (CFD) for patient-specific geometry to investigate the influence of severe angular ($\geq$ 60°) neck on AAA's hemodynamic and wall shear stress. The patient's geometrical characteristics were obtained from a computed tomography images database of AAA patients. The AAA geometry was reconstructed using Mimics software. In computational method, blood was assumed Newtonian fluid and an inlet varying velocity waveform in a cardiac cycle was assigned. The CFD study was performed with ANSYS software. The results of flow behaviours indicated that the blood flow through severe bending of angular neck leads to high turbulence and asymmetry of flows within the aneurysm sac resulting in blood recirculation. The high wall shear stress (WSS) occurred near the AAA neck and on surface of aneurysm sac. This study explained and showed flow behaviours and WSS progression within high angular neck AAA and risk predication of abdominal aorta rupture. We expect that the visualization of blood flow and hemodynamic changes resulted from CFD simulation could be as an extra tool to assist clinicians during a decision making when estimation the risks of interventional procedures.

Keywords: Computational fluid dynamics; Abdominal aortic aneurysm; Wall shear stress; Hemodynamic, Computed tomography

3

List of symbols

3D   Three-dimensional

AAAs   Abdominal aortic aneurysms

CAD   Computer-aided design

CFD   Computational fluid dynamics

CT   Computed tomography

CVD   Cardiovascular disease

DICOM   Digital imaging and communications in medicine

EVAR   Endovascular aortic aneurysm repair

ILT   Intraluminal thrombus

MR   Magnetic resonance

ROI   Region of interest

STL   Stereolithography

UDF   User-defined function

WSS   Wall shear stress

1 Introduction

Cardiovascular disease (CVD) is one of the foremost common cause of global mortality rate [1]. In 2013, a report of Global Burden of Disease stated that 17.3 million cases of death caused by CVD globally, which accounted approximately 31.5% of total deaths [1, 2]. One of most prevalent cardiovascular diseases is abdominal aortic aneurysm (AAA) [3]. Abdominal aortic aneurysm is defined as a dilatation of the artery that located below the renal arteries[4, 5], with at least a diameter of 30 mm or about 1.5 times the normal size of aorta [6]. Abdominal aortic aneurysms are often diagnosed through the presence of intraluminal thrombus deposition and are linked to the degradation of the connective tissue in the arterial

wall, which made up of cell debris and fibrinous blood clots [7]. Abdominal aortic aneurysms are formed due to several mechanisms including, inflammation of immune responses and aortic wall degradation, which are affected by molecular genetics [8, 9]. During the aneurysm formation, a complex blood flow environment and altered wall shear stress distribution are induced. Moreover, AAA is considered life-threatening health condition, which can require urgent surgical intervention [7]. Continuous AAA expansion leads to the decline of aortic wall strength, in which case the wall becomes susceptible to collapse or eventual aortic rupture [10]. Current clinical recommendations are that; when the AAA diameters reach 55 mm in men and 50 mm in women, with a development rate of 8.0 mm/year, then surgical intervention is necessary [5, 10].

Currently, the intervention process is either in a form of open surgery or endovascular repair based on diameter size of aneurysm sac with a follow up routines every six months or yearly [11, 12]. However, the aneurysm diameter is still a poor indicator of rupture since some reported aneurysms with larger diameter remain intact, while aneurysms of a smaller size have been reported to rupture [5, 10, 13]. Thus, AAA rupture is ranked as the 13th leading cause of mortality in the US alone with approximately 15,000 patients every year, and reports of more than 8,000 cases of death in the UK [7, 14]; further, AAAs as regards surgical emergencies, the mortality rate as high as 90% [15]. The numerous studies conducted on the prediction of rupture and its risks, have proposed several possible AAA rupture factors including asymmetry flow index, maximum aneurysm diameter, age, aortic wall stiffness, mechanical stress, aneurysm growth rate, intraluminal thrombus ratio, smoking, hypertension and high cholesterol [8, 11, 16–18]. However, morphologies such as aortic neck angulation related to adverse events and outcome after endovascular abdominal aortic aneurysm repair **[19]** have often been overlooked**.**

Generally, magnetic resonance (MR) and a computer tomography (CT) can be used to obtain the anatomy of cardiovascular structures [20]. The resulting images of vasculature are valuable to generate numerical models which can be used to predict mechanical behavior under these conditions. Thus, Computational fluid dynamics (CFD) has been used for cardiovascular research, including flow analysis and calculation of wall shear stress [21–24]. For the study of AAAs, CFD has been implemented in the applications of idealized or patient-specific geometries to assist in predicting the rupture risks [25, 26]. Several studies indicated that wall stresses depend on the particular curvatures and a non-symmetric aneurysm wall which can be useful to predict the rupture site [12, 27–32]; thus, highly patient specific. There is the potential to address the paucity of research into the influence of neck angulation on AAA disease progression and AAA risk of rupture, through the use of a numerical model.

The aim of this present study, is to develop a three-dimensional finite volume method for CFD simulation, focusing on the impact of proximal aneurysm neck angulations on the blood flow within the aorta and wall shear stress (WSS) this angulation has been assessed in this numerical study, using patient-specific AAA geometry.

2 Materials and Methods

2.1 Image acquisition

The three-dimensional (3D) vasculature was based on CT images of the angular neck of a single patient with AAA was fully analysed. These images were acquired from radiology department under the approval of Faculty of Medicine Ethics Committee, Prince of Songkla University with number (REC.61-010-25-2). The CT images were obtained in a DICOM format by AQUILION PRIME (Toshiba, Japan) with single slices, rows and columns of 512

x 512 pixels, a slice thickness of 3 mm and mean pixel spacing of 0.669 x 0. 669. Table 1 presents patient's demographic information, including angle at proximal neck.

2.2 Three-Dimensional Model Reconstruction

The Three-dimensional (3D) smoothed model was generated from DICOM files by using the commercial medical imaging software Mimics v18.0 (Materialise, Belgium). Mimics was used to convert the acquired CT images into a patient specific 3D CAD model. The region of interest (ROI) was segmented by applying grayscale-based thresholding tools. The DICOM images were cropped from the position of the infra-renal aorta towards the bifurcation of common iliac arteries. The artery branches such as parietal and visceral arteries were excluded from the reconstruction to simplify the geometries. Examples of the thresholding and segmentation processes are shown in figure 1(a) and 1(b). Finally, the 3D smoothed geometry was generated and exported as a binary 'STL (stereolithography)' format as shown in figure 1(c). The proximal neck angulation of patient's specific model was measured by using Mimics, with measurement provided in Table 1.

2.3 Meshing

The geometry was meshed by using the Octree method in ANSYS ICEM v16.2 (ANSYS Inc., USA) for tetrahedral meshing. An inflation at the wall boundary was implemented with five prism layers. The height of first layer was set to 0.1 mm, and next layers grow with a size ratio of 1.2. Quality and smoothing checks were repeatedly performed to ensure a satisfactory mesh. A grid-size independency study was performed using a ±2.5% for peak velocity as the key criterion. The final mesh has 2,077,498 elements.

2.4 Boundary conditions and material properties

A finite volume method was implemented to solve the Navier-Stokes and continuity equations of the fluid motion under transient conditions in ANSYS FLUENT v16.2 (ANSYS Inc., USA) [33] solver. Blood flow was assumed to be homogeneous, incompressible, and blood was modelled as a Newtonian fluid. These assumptions are adequate in larger arteries with a constant dynamic viscosity and blood density of 0.0035 Pa·s and 1,060 kg/m^3, respectively [34–36]. Furthermore, an assumption of flow in aorta with > 0.5 mm diameter as Newtonian is acceptable since the viscosity of blood is comparatively constant at the high shear rates (100/s), and this case is typically found in abdominal aortas [37, 38]. For the fluid domain, the flow of blood in vessels and arteries are pulsatile [39]. Thus, a user-defined function (UDF) for a pulsatile velocity profile was used at the inlet for the whole cardiac pulse cycle with a velocity magnitude between 0 and 0.3 m/s as shown in figure 2. The inlet velocity profile was adopted from Rissland *et al.*[10]. For the outlet boundary, a fully developed outflow of a zero diffusion flux boundary condition was applied at the common iliac arteries [36, 40]. A no-slip wall condition on the arterial walls was assumed.

2.5 Simulation setup

All CFD transient simulations to solve the Navier-Stokes equations were carried out using ANSYS FLUENT v16.2 (ANSYS Inc.) under the k-omega (*k-ω*) turbulence model with a second order implicit method for transient formulations. The pressure-velocity coupling was set as SIMPLE algorithm to solve the continuity equation under 2nd order upwind momentum for spatial discretization. The convergence criteria for the normalized continuity and velocity residuals were 1×10^{-5}. A fixed time step of 0.01s was used and three cardiac cycles (3×0.94s) =2.82s or 282 time-steps were completed for each simulation.

3 Results and Discussion

The unsteady results of flow patterns (velocity contours in cross-sectional areas and streamlines) and WSS are presented at four different time points of a cardiac cycle indicated by the points in figure 2. These times are (a) peak systole t = 0.25 s, (b) early diastole t = 0.55 s, (c) mid-diastole t = 0.70 s, and (d) late diastole t = 0.94 s.

3.1 Flow patterns

The velocity contours in regions of interest are presented in both horizontal and longitudinal cross-sectional areas as can be seen in figure 3(a). Four horizontal cross-sectional slides (A, B, D and C) in figure 3(b), and one longitudinal cross-sectional slide (E) extended from upper neck region towards the distal area of the sac as in figure 3(c). The contours of velocity within the horizontal cross-sectional slides show that the magnitude of velocity is significantly changed over the time. The maximum velocity at the peak systole clearly seems to be higher by approximately 55% than other maximum velocities over the different time points in a cardiac cycle, while velocity flow among the diastolic stages show similarity with very difference of only 4%. However, at all four time-points of a cardiac cycle the maximum blood flow appeared to be occur near the inner wall of the aorta, but cross-section of slide D views maximum blood flow near both inner and outer walls with local average velocity (0.15 m/s). The flows within slides C and D tend to form a circular shape within the aortic sac that can cause a high blood recirculation while maintaining a low velocity at the center of aorta with approximately 0.04 m/s.

In the region of longitudinal cross-section, figure 3c emphasizes on the velocity flow starting from upper the neck bending region towards the distal sac of aneurysm represented by the square box for the ROI. The contour at peak systole 0.25 s shows an arch shape of thin

bar of velocity flow entering the proximal neck of aneurysm towards the sac and forming a

9

bulk of blood flow near the outer wall of aorta, while it diminishes gradually over variant times through diastolic flow. At a full cardiac cycle 0.94 s, the flow in the aneurysm sac generates an interesting form of flow which can be clearly seen at the inner and outer sides of the artery wall.

The streamlines of velocity flows are presented in figure 4. The swirling of instantaneous velocity streamlines were acquired at different time points of a cardiac cycle. Distinguished lines of flows are displayed for ROI around the angular neck AAA. The recirculation blood vortexes are easily recognizable in various patterns over time.

3.2 WSS distribution

The WSS distribution of four different time points of a cardiac cycle configuration (peak systole, early diastole, mid diastole and late diastole) for highly proximal neck angulation of AAA is depicted in figure 5. The WSS distributions are illustrated in three different views. View 1 and 2 show the WSS in the inner and outer sides of the neck region, while view 3 illustrates the WSS distribution on the surface of aneurysm sac. We can observe that the high WSS of 1.24 Pa occurs at the area of proximal neck due to the turbulent flow exhibited within the region of angulation. The high bending, the severe tortuosity of aortic surface and asymmetric blood flow seem to be possible indicators of WSS and aortic rupture. At the peak systole and a fully developed cardiac cycle as in figure 6, high WSS regions are located at the areas below the angular neck and over the aneurysm sac as indicated by the red arrows with average value of 0.94 Pa, while the locations of low WSS with the average of 0.077 Pa are indicated by the black arrows.

In this study, three-dimensional computational fluid dynamics simulations of a bending angulation neck of patient-specific AAA have been used to assess time-dependent hemodynamic. The three-dimensional geometry of angular neck AAA was reconstructed

from computed tomography images. More specifically, the impact of high angular neck AAA on blood flow and wall shear stress (WSS) were assessed for a bending angle (>60°); particularly important due to the lack of studies in this area [19], with previous studies focused on smaller proximal angles (≤ 60°) or using idealized geometries [6, 14, 19, 40, 41].

3.3 Hemodynamic changes

Our study demonstrated the hemodynamic changes occur more pronounce at peak systole and turbulence flow was generated at the neck throughout the sac during a cardiac cycle. In this study, the presence of a bending angle greater than 60° caused high flow turbulence and irregularities of blood-flow streamlines. This indicates that WSS and their distribution will be altered, with potential impact on weakening of arteries wall [40, 41].

The flow patterns at the systolic stage were observed to have complex and high velocity values within the proximal neck, while these maximum velocity values seemed to be decreased at the early and mid-diastole stages before it increased again during the complete full cardiac cycle. The impact of proximal angular neck on the flow within aneurysm sac was clearly showed to form a complex recirculation and flow impingement. This impact demonstrated a clear difference between the flow in AAA with proximal neck and without proximal neck as reported in previous study for AAA [42] where the blood flows within the aneurysm sac were presented and visualized to be straight streamlines with very small region of recirculation due to the existing of aneurysm. However, the results showed that the velocity flow within the aorta observed to have vorticity flow and recirculation particularly through the aneurysm sac and aortic bifurcation, and these findings are consistent with idealized geometries in prior studies [26, 40, 41, 43], but our study reveals more complex recirculation and vorticity due to highly angulated neck and complexity of patient specific

AAA geometry. Furthermore, a larger diameter for ruptured AAAs was associated with

11

greater recirculation flow whereas less recirculation was found in smaller ruptured AAAs [44].

Several factors that influence the hemodynamic and the biomechanical conditions of arteries in cardiovascular system. For instance, vascular geometry [45], elasticity of the wall, blood viscosity and pathological conditions [46]. Xenos et al.[14] conducted numerical simulations for 26 idealized geometries based on patient-specific data by using Fluid-Structure Interaction simulations to investigate the effect of proximal necks (40.10±16.30°) in AAA. Correspondingly, Drewe et al. [6] studied similar range of neck angles in Xenos et al.[14] for idealized geometries in order to observe the stresses and hemodynamics. Both reported that peak WSS seems to be increased with the increase of proximal neck angles. However, the smaller angle of necks in their studies predicted peak WSS in the middle region of aneurysm sac due to the less turbulence of blood flow generated, while our findings with a larger neck showed WSS can be located more diffuse across areas such as below the proximal neck, middle of sac as well as at the lower side of the aneurysm sac wall. It has been reported that high WSS can promote endothelial injury [47] while low WSS can lead to inflammatory infiltration [48]. Therefore, this study has predicted a link between the behavior of blood flow and the change of WSS distribution. This correlation is consistent, and demonstrates agreement with a previous study conducted by Arzani and Shadden [49].

The k-ω model was used in this study according to both Banks et al.[50] and Ryval et al.[51] who found that this model was preferred for CFD turbulent flow simulations in arteries due to its better performances from other turbulence models when comparing the simulation outcomes against the results of experimental data. Furthermore, the k-ω model showed a good performance for the flow at boundary layers close to the wall, without applying a function of wall enhancement [50]. Therefore, it was observed that k-ω model was

the most suitable method that provides better comparisons against the experimental results [51], it can be used for transitional flows for low Reynolds number.

3.4 Limitation of study

The findings of this work may have some limitations since only one angular neck of AAA patient-specific geometry was carried out for this simulation. However, it demonstrates the effect of geometrical features based on realistic time-varying velocity waveform, which is can be considered for personalized healthcare. It is appropriate also to mention that this study implemented outflow boundary conditions at outlets which used the same waveform at the inlet of AAA section. This assumption is not expected to alter the overall findings as regards AAA neck angle and altered hemodynamics. Furthermore, it is worthy to point out that a possible thrombus was not included in this study. The presence of intraluminal thrombus (ILT) encourages the change of geometrical features that can consequently influence the biomechanics of AAA [52]. However, ILT was not involved in a scope of our study.

4 Conclusions

To summarize this work, the simulation concluded that the tortuosity of the aortic neck angulation causes a downstream of blood flow to be a turbulent flow and leads a weakening of the aortic wall, resulting in forming locations of high WSS. Thus, this study presented a comprehensive idea on the behavior of blood flow in highly angulated abdominal aortic aneurysm necks and its influence on wall shear stress. Furthermore, we recommend that more realistic geometries are necessary to study the effect of angularity of neck on blood flow behaviors and hemodynamic changes.

References

1. Townsend, N.; Wilson, L.; Bhatnagar, P.; Wickramasinghe, K.; Rayner, M.; Nichols, M.: Cardiovascular disease in Europe: Epidemiological update 2016. Eur. Heart J. **37**, 3232–3245 (2016). doi:10.1093/eurheartj/ehw334

2. Barquera, S.; Pedroza-Tobías, A.; Medina, C.; Hernández-Barrera, L.; Bibbins-Domingo, K.; Lozano, R.; Moran, A.E.: Global Overview of the Epidemiology of Atherosclerotic Cardiovascular Disease. Arch. Med. Res. **46**, 328–338 (2015). doi:10.1016/j.arcmed.2015.06.006

3. Dua, M.M.; Dalman, R.L.: Hemodynamic Influences on abdominal aortic aneurysm disease: Application of biomechanics to aneurysm pathophysiology. Vascul. Pharmacol. **53**, 11–21 (2010). doi:10.1016/j.vph.2010.03.004

4. Humphrey, J.D.; Holzapfel, G.A.: Mechanics, mechanobiology, and modeling of human abdominal aorta and aneurysms. J. Biomech. **45**, 805–814 (2012). doi:10.1016/j.jbiomech.2011.11.021

5. Lozowy, R.J.; Kuhn, D.C.S.S.; Ducas, A.A.; Boyd, A.J.: The Relationship Between Pulsatile Flow Impingement and Intraluminal Thrombus Deposition in Abdominal Aortic Aneurysms. Cardiovasc. Eng. Technol. **8**, 57–69 (2017). doi:10.1007/s13239-016-0287-5

6. Drewe, C.J.; Parker, L.P.; Kelsey, L.J.; Norman, P.E.; Powell, J.T.; Doyle, B.J.: Haemodynamics and stresses in abdominal aortic aneurysms: A fluid-structure interaction study into the effect of proximal neck and iliac bifurcation angle. J. Biomech. **60**, 150–156 (2017). doi:10.1016/j.jbiomech.2017.06.029

7. Raut, S.S.; Chandra, S.; Shum, J.; Finol, E.A.: The role of geometric and biomechanical factors in abdominal aortic aneurysm rupture risk assessment. Ann. Biomed. Eng. **41**, 1459–1477 (2013). doi:10.1007/s10439-013-0786-6

14

8. Arzani, A.; Suh, G.-Y.; Dalman, R.L.; Shadden, S.C.: A longitudinal comparison of hemodynamics and intraluminal thrombus deposition in abdominal aortic aneurysms. Am. J. Physiol. Circ. Physiol. **307**, H1786–H1795 (2014). doi:10.1152/ jpheart.00461.2014

9. Ailawadi, G.; Eliason, J.L.; Upchurch, G.R.: Current concepts in the pathogenesis of abdominal aortic aneurysm. J. Vasc. Surg. **38**, 584–588 (2003). doi:10.1016/S0741-5214(03)00324-0

10. Rissland, P.; Alemu, Y.; Einav, S.; Ricotta, J.; Bluestein, D.: Abdominal Aortic Aneurysm Risk of Rupture: Patient-Specific FSI Simulations Using Anisotropic Model. J. Biomech. Eng. **131**, 31001 (2009). doi:10.1115/1.3005200

11. Kleinstreuer, C.; Li, Z.: Analysis and computer program for rupture-risk prediction of abdominal aortic aneurysms. Biomed. Eng. Online. **5**, 5–19 (2006). doi:10.1186/1475-925X-5-19

12. Li, Z.; Kleinstreuer, C.: A new wall stress equation for aneurysm-rupture prediction. Ann. Biomed. Eng. **33**, 209–213 (2005). doi:10.1007/s10439-005-8979-2

13. Giuma, S.K.B.; Osman, K.; Kadir, M.R.A.: Fluid Structure Interaction Analysis in Abdominal Aortic Aneurysms: Influence of Diameter, Length, and Distal Neck. J. Med. Imaging Heal. Informatics. **3**, 514–522 (2013). doi:10.1166/jmihi.2013.1201

14. Xenos, M.; Alemu, Y.; Zamfir, D.; Einav, S., Ricotta, J.J.; Labropoulos, N.; Tassiopoulos, A.; Bluestein, D.: The effect of angulation in abdominal aortic aneurysms: Fluid-structure interaction simulations of idealized geometries. Med. Biol. Eng. Comput. **48**, 1175–1190 (2010). doi:10.1007/s11517-010-0714-y

15. Assar, A.N.; Zarins, C.K.: Ruptured abdominal aortic aneurysm: A surgical emergency with many clinical presentations. Postgrad. Med. J. **85**, 268–273 (2009). doi:10.1136/pgmj.2008.074666

16. Van Damme, H.; Sakalihasan, N.; Limet, R.: Factors promoting rupture of abdominal aortic aneurysms. Acta Chir. Belg. **105**, 1–11 (2005)

17. Wolf, Y.G.; Thomas, W.S.; Brennan, F.J., Goff, W.G.; Sise, M.J.; Bernstein, E.F.: Computed tomography scanning findings associated with rapid expansion of abdominal aortic aneurysms. J. Vasc. Surg. **20**, 529–538 (1994). doi:10.1016/0741-5214(94)90277-1

18. Blanchard, J.F.: Epidemiology of abdominal aortic aneurysms. Epidemiol Rev. **21**, 207–221 (1999). doi:10.1093/oxfordjournals.epirev.a017997

19. Sternbergh, W.C.; Carter, G.; York, J.W.; Yoselevitz, M.; Money, S.R.: Aortic neck angulation predicts adverse outcome with endovascular abdominal aortic aneurysm repair. J. Vasc. Surg. **35**, 482–486 (2002). doi:10.1067/mva.2002.119506

20. Gray, R.A.; Pathmanathan, P.: Patient-Specific Cardiovascular Computational Modeling: Diversity of Personalization and Challenges. J. Cardiovasc. Transl. Res. **11**, 1–9 (2018). doi:10.1007/s12265-018-9792-2

21. Morris, P.D.; Narracott, A.; Von Tengg-Kobligk, H.; Soto, D.A.S.; Hsiao, S.; Lungu, A., Evans, P.; Bressloff, N.W.; Lawford, P. V.; Rodney Hose, D.; Gunn, J.P.: Computational fluid dynamics modelling in cardiovascular medicine. Heart. **102**, 18–28 (2016). doi:10.1136/heartjnl-2015-308044

22. Chung, B.; Cebral, J.R.: CFD for Evaluation and Treatment Planning of Aneurysms: Review of Proposed Clinical Uses and Their Challenges. Ann. Biomed. Eng. **43**, 122–138 (2014). doi:10.1007/s10439-014-1093-6

23. Tseng, F.S.; Soong, T.K.; Syn, N.; Ong, C.W.; Liangb, L.H.; Choongc, A.M.T.L.: Computational fluid dynamics in complex aortic surgery: applications, prospects and challenges. J. Surg. Simul. **4**, 1–4 (2017). doi:10.1102/2051-7726.2017.0001

24. van Bakel, T.M.J.; Lau, K.D.; Hirsch-Romano, J.; Trimarchi, S.; Dorfman, A.L.;

Figueroa, C.A.: Patient-Specific Modeling of Hemodynamics: Supporting Surgical Planning in a Fontan Circulation Correction. J. Cardiovasc. Transl. Res. **11**, 1–11 (2018). doi:10.1007/s12265-017-9781-x

25.   Carty, G.; Chatpun, S.; Espino, D.M.: Modeling Blood Flow Through Intracranial Aneurysms: A Comparison of Newtonian and Non-Newtonian Viscosity. J. Med. Biol. Eng. **36**, 396–409 (2016). doi:10.1007/s40846-016-0142-z

26.   Owen, B.; Lowe, C.; Ashton, N.; Mandal, P.; Rogers, S.; Wein, W.; McCollum, C.; Revell, A.: Computational hemodynamics of abdominal aortic aneurysms: Three-dimensional ultrasound versus computed tomography. Proc. Inst. Mech. Eng. Part H J. Eng. Med. **230**, 201–210 (2016). doi:10.1177/0954411915626742

27.   Raghavan, M.L.; Vorp, D.A.; Federle, M.P.; Makaroun, M.S.; Webster, M.W.: Wall stress distribution on three-dimensionally reconstructed models of human abdominal aortic aneurysm. J. Vasc. Surg. **31**, 760–769 (2000). doi:10.1067/mva.2000.103971

28.   del Álamo, J.C.; Marsden, A.L.; Lasherasa, J.C.: Recent Advances in the Application of Computational Mechanics to the Diagnosis and Treatment of Cardiovascular Disease. Rev. Española Cardiol. (English Ed. **62**, 781–805 (2009). doi:10.1016/S1885-5857(09)72359-X

29.   Fillinger, M.F.; Marra, S.P.; Raghavan, M.L.; Kennedy, F.E.: Prediction of rupture risk in abdominal aortic aneurysm during observation: Wall stress versus diameter. J. Vasc. Surg. **37**, 724–732 (2003). doi:10.1067/mva.2003.213

30.   Di Martino, E.S.; Vorp, D.A.: Effect of variation in intraluminal thrombus constitutive properties on abdominal aortic aneurysm wall stress. Ann. Biomed. Eng. **31**, 804–809 (2003). doi:10.1114/1.1581880

31.   Raghavan, M.L.; Fillinger, M.F.; Marra, S.P.; Naegelein, B.P.; Kennedy, F.E.: Automated Methodology for Determination of Stress Distribution in Human

Abdominal Aortic Aneurysm. J. Biomech. Eng. **127**, 868–871 (2005). doi:10.1115/1.1992530

32.   Di Martino, E.S.; Guadagni, G.; Fumero, A.; Ballerini, G.; Spirito, R.; Biglioli, P.; Redaelli, A.: Fluid-structure interaction within realistic three-dimensional models of the aneurysmatic aorta as a guidance to assess the risk of rupture of the aneurysm. Med. Eng. Phys. **23**, 647–655 (2001). doi:10.1016/S1350-4533(01)00093-5

33.   Morbiducci, U.; Ponzini, R.; Gallo, D.; Bignardi, C.; Rizzo, G.: Inflow boundary conditions for image-based computational hemodynamics: Impact of idealized versus measured velocity profiles in the human aorta. J. Biomech. **46**, 102–109 (2012). doi:10.1016/j.jbiomech.2012.10.012

34.   Morris, L.; Delassus, P.; Callanan, A.; Walsh, M.; Wallis, F.; Grace, P.; McGloughlin, T.: 3-D Numerical Simulation of Blood Flow Through Models of the Human Aorta. J. Biomech. Eng. **127**, 767–775 (2005). doi:10.1115/1.1992521

35.   Renner, J.; Loyd, D.; Länne, T.; Karlsson, M.: Is a flat inlet profile sufficient for WSS estimation in the aortic arch? WSEAS Trans. Fluid Mech. **4**, 148–160 (2009)

36.   Morbiducci, U.; Gallo, D., Massai, D.; Consolo, F.; Ponzini, R., Antiga, L.; Bignardi, C.; Deriu, M. a.; Redaelli, A.: Outflow conditions for image-based hemodynamic models of the carotid bifurcation: implications for indicators of abnormal flow. J. Bomechanical Eng. **132**, 91005 (2010). doi:10.1115/1.4001886

37.   Scotti, C.M.; Finol, E.A.: Compliant biomechanics of abdominal aortic aneurysms: A fluid-structure interaction study. Comput. Struct. **85**, 1097–1113 (2007). doi:10.1016/j.compstruc.2006.08.041

38.   Frauenfelder, T.; Lotfey, M.; Boehm, T.; Wildermuth, S.: Computational fluid dynamics: Hemodynamic changes in abdominal aortic aneurysm after stent-graft implantation. Cardiovasc. Intervent. Radiol. **29**, 613–623 (2006). doi:10.1007/s00270-

18

005-0227-5

39. ChungDann Kan, T.C.: Numerical Simulation of Blood Flow in Double-Barreled Cannon EVAR and its Clinical Validation. J. Vasc. Med. Surg. **2**, (2014). doi:10.4172/2329-6925.1000160

40. Yeow, S.L.; Leo, H.L.: Hemodynamic Study of Flow Remodeling Stent Graft for the Treatment of Highly Angulated Abdominal Aortic Aneurysm. Comput. Math. Methods Med. **2016**, 1–10 (2016). doi:10.1155/2016/3830123

41. Algabri, Y.A.; Rookkapan, S.; Chatpun, S.: Three-dimensional finite volume modelling of blood flow in simulated angular neck abdominal aortic aneurysm. IOP Conf. Ser. Mater. Sci. Eng. **243**, 12003 (2017). doi:10.1088/1757-899X/243/1/012003

42. Finol, E.A.; Keyhani, K.; Amon, C.H.: The Effect of Asymmetry in Abdominal Aortic Aneurysms Under Physiologically Realistic Pulsatile Flow Conditions. J. Biomech. Eng. **125**, 207–217 (2003). doi:10.1115/1.1543991

43. Shek, T.L.T.; Tse, L.W.; Nabovati, A.; Amon, C.H.: Computational Fluid Dynamics Evaluation of the Cross-Limb Stent Graft Configuration for Endovascular Aneurysm Repair. J. Biomech. Eng. **134**, 121002 (2012). doi:10.1115/1.4007950

44. Boyd, A.J.; Kuhn, D.C.S.; Lozowy, R.J.; Kulbisky, G.P.: Low wall shear stress predominates at sites of abdominal aortic aneurysm rupture. J. Vasc. Surg. **63**, 1613–1619 (2016). doi:10.1016/j.jvs.2015.01.040

45. Gounley, J.; Vardhan, M.; Randles, A.: A Computational Framework to Assess the Influence of Changes in Vascular Geometry on Blood Flow. In: Proceedings of the Platform for Advanced Scientific Computing Conference on - PASC '17. pp. 1–8. , Lugano (2017)

46. Sinnott, M.; Cleary, P.W.; Prakash, M.: An investigation of pulsatile blood flow in a bifurcation artery using a grid-free method. In: Proc. Fifth International Conference on

CFD in the Process Industries. pp. 1–6. , Melbourne (2006)

47. Langille, B.L.; O'Donnell, F.: Reductions in arterial diameter produced by chronic decreases in blood flow are endothelium-dependent. Science (80-.). **231**, 405–407 (1986). doi:10.1126/science.3941904

48. Zarins, C.K.; Giddens, D.P.; Bharadvaj, B.K.; Sottiurai, V.S.; Mabon, R.F.; Glagov, S.: Carotid bifurcation atherosclerosis. Quantitative correlation of plaque localization with flow velocity profiles and wall shear stress. Circ. Res. **53**, 502–514 (1983). doi:10.1161/01.RES.53.4.502

49. Arzani, A.; Shadden, S.C.: Characterizations and Correlations of Wall Shear Stress in Aneurysmal Flow. J. Biomech. Eng. **138**, 14503 (2015). doi:10.1115/1.4032056

50. Banks, J.; Bressloff, N.W.: Turbulence Modeling in Three-Dimensional Stenosed Arterial Bifurcations. J. Biomech. Eng. **129**, 40–50 (2007). doi:10.1115/1.2401182

51. Ryval, J.; Straatman, A.G.; Steinman, D.A.: Two-equation Turbulence Modeling of Pulsatile Flow in a Stenosed Tube. J. Biomech. Eng. **126**, 625–635 (2004). doi:10.1115/1.1798055

52. Deplano, V.; Knapp, Y.; Bailly, L.; Bertrand, E.: Flow of a blood analogue fluid in a compliant abdominal aortic aneurysm model: Experimental modelling. J. Biomech. **47**, 1262–1269 (2014). doi:10.1016/j.jbiomech.2014.02.026

Table1: Patient demographics and geometrics information.

Patient's information	
Gender	Male
Age, yrs	74
Weight	65
Height	158
Inflow inlet diameter (mm)	25
Proximal Neck diameter (mm)	20
Infrarenal Neck length (mm)	25
Aneurysm length (mm)	68
Aneurysm diameter (mm)	56
Distal left iliac diameter (mm)	8
Distal right iliac diameter (mm)	8
Angle at Proximal neck	79º
Whole model length (mm)	258.06

Figure legends

Fig. 1 Overall geometry reconstructions process, (a) computer tomography image for the whole aorta, (b) the thresholding mask for aorta in the axial, coronal and sagittal view, and (c) three dimensional geometry for AAA after reconstruction.

Fig. 2 Velocity waveform profile imposed at the inlet. (a) peak systole at 0.25 s; (b) early diastole 0.55 s; (c) mid diastole 0.70 s; and (d) late diastole 0.94 s.

Fig. 3 Velocity contours at different horizontal cross-sectional areas for the angular neck AAA and aortic sac indicated by letters: (a) the four different locations in the geometry; (b) comparisons of the magnitude of the flow velocity at different time points in a cardiac cycle; (c) the vertical cross-sectional area of the model from proximal neck to lower region of sac.

Fig. 4 Flow streamline contours at four different time points in a cardiac cycle.

Fig. 5 Wall shear stress (WSS) distribution on the angular neck and aneurysm sac regions at different time points in a cardiac cycle.

Fig. 6 Wall shear stress (WSS) distribution for two time-points in a cardiac cycle as prescribed by the graph. The high WSS regions are located with red arrows with average value of 0.94 Pa, while the locations of low WSS with the average of 0.077 Pa are indicated by the black arrows.

Cover Letter

June 23, 2018

Dear Editor:

My coauthors and I would like to submit the enclosed manuscript, *"Computational study on hemodynamic changes in patient-specific proximal neck angulation of abdominal aortic aneurysm with time-varying velocity"* for publication in *"Arabian Journal for Science and Engineering"*. This work we showed that how angulation of neck in abdominal aneurysm effect on blood flow behavior and shear stress on aneurysm wall using real geometry from patient that can make more understand to clinician. Furthermore, this result can assist the clinician to plan for the intervention treatment.

We confirm that this manuscript has not been under reviewed to any journals.

We would be grateful if the manuscript could be reviewed and considered for publication in *"Arabian Journal for Science and Engineering"*.

We look forward to hearing from you.

Very sincerely yours,

Surapong Chatpun

Surapong Chatpun
Institute of Biomedical Engineering, Faculty of Medicine
Prince of Songkla University, Thailand 90110
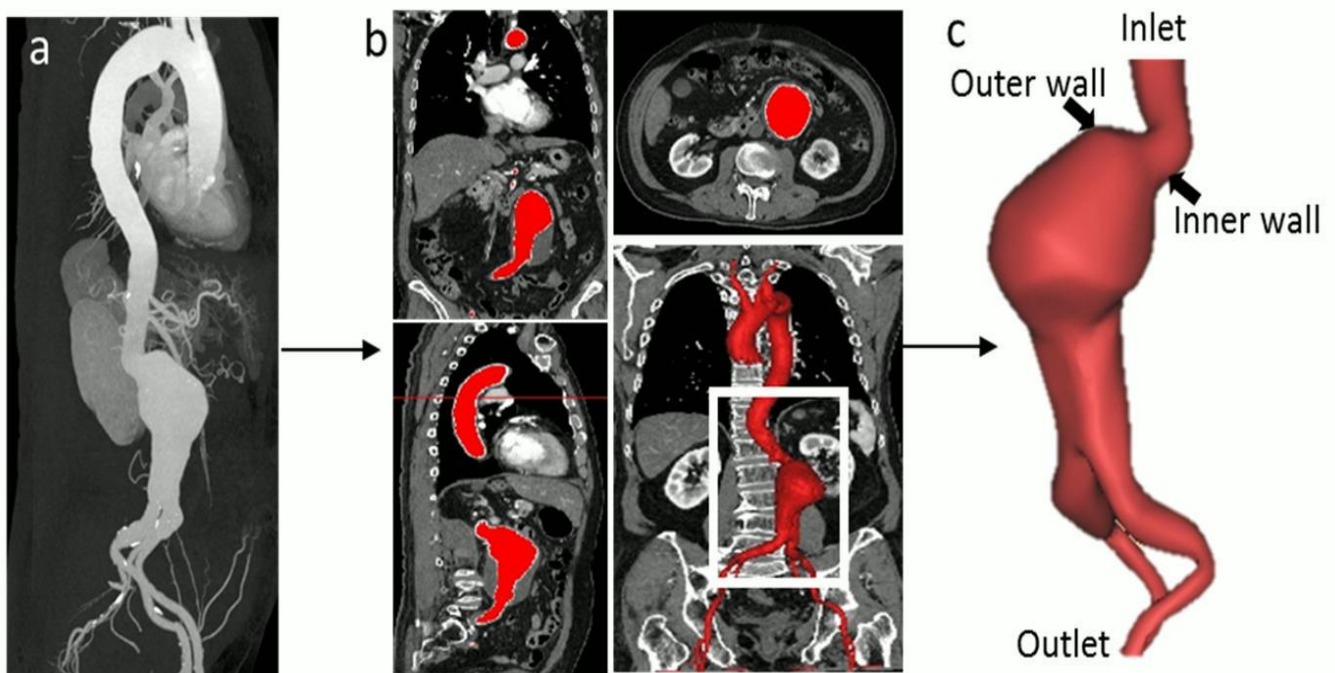Tel: 66-7445-1743, Fax: 66-7445-1744   Email: surapong.c@psu.ac.th

Fig. 1: Overall geometry reconstructions process, (a) CT image for the whole aorta, (b) the thresholding mask for aorta in the axial, coronal and sagittal view, and (c) 3D geometry for AAA after reconstruction.
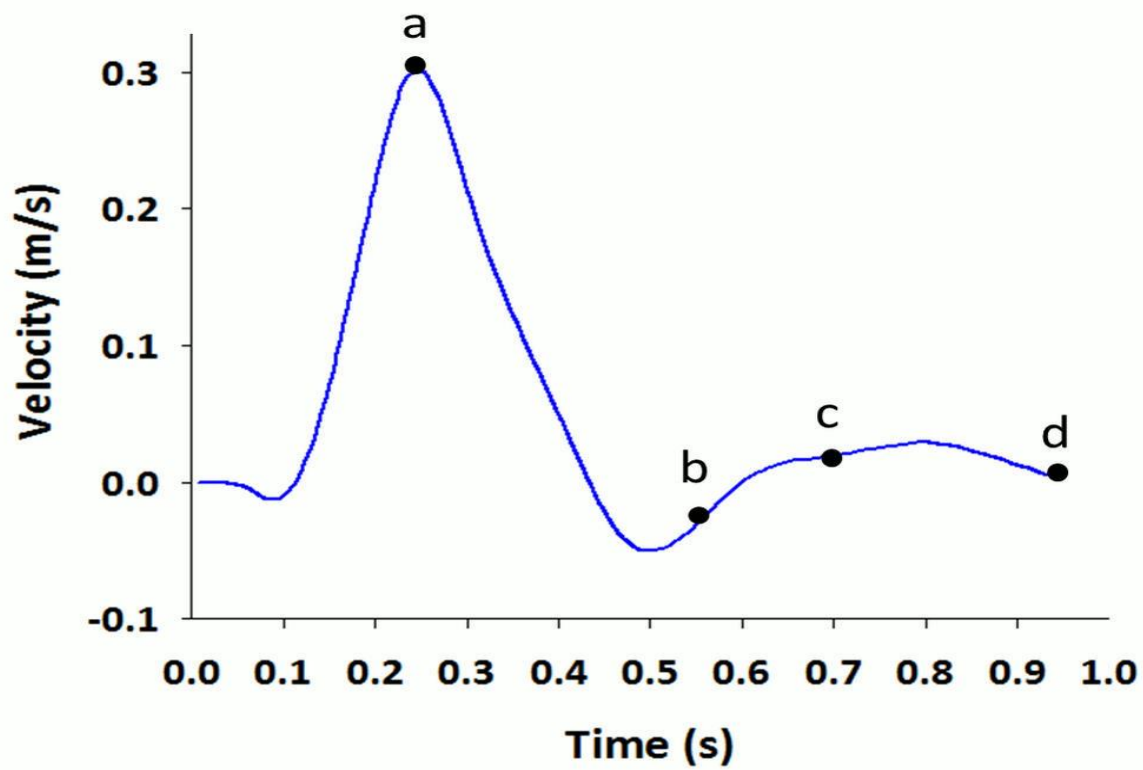
Fig. 2: Velocity waveform profile imposed at the inlet. (a) peak systole at 0.25 s; (b) early diastole 0.55 s; (c) mid diastole 0.70 s; and (d) late diastole 0.94 s.
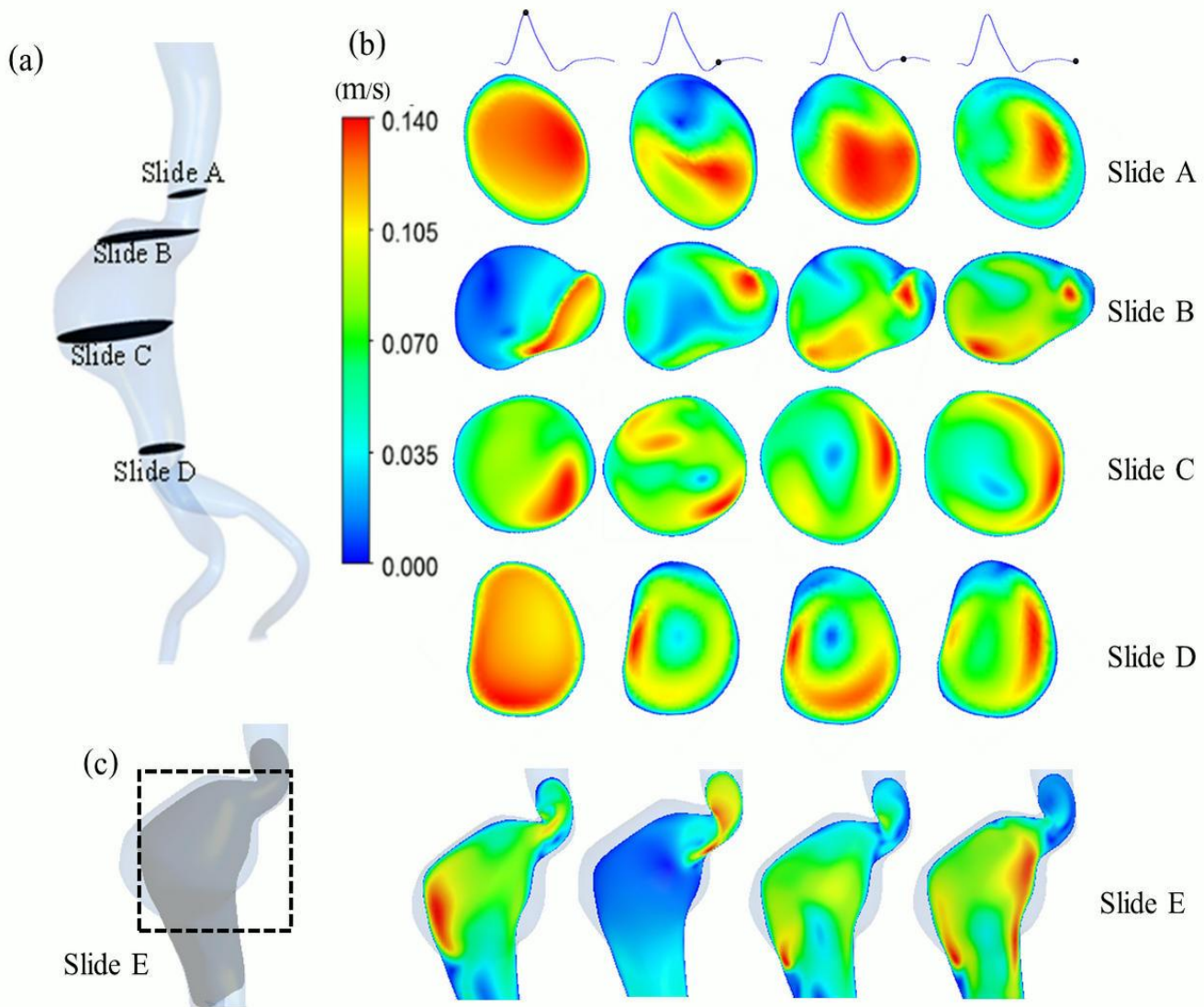
Fig. 3: Velocity contours at different horizontal cross-sectional areas for the angular neck AAA and aortic sac indicated by letters: (a) the four different locations in the geometry; (b) comparisons of the magnitude of the flow velocity at different time points in a cardiac cycle; (c) the vertical cross-sectional area of the model from proximal neck to lower region of sac.
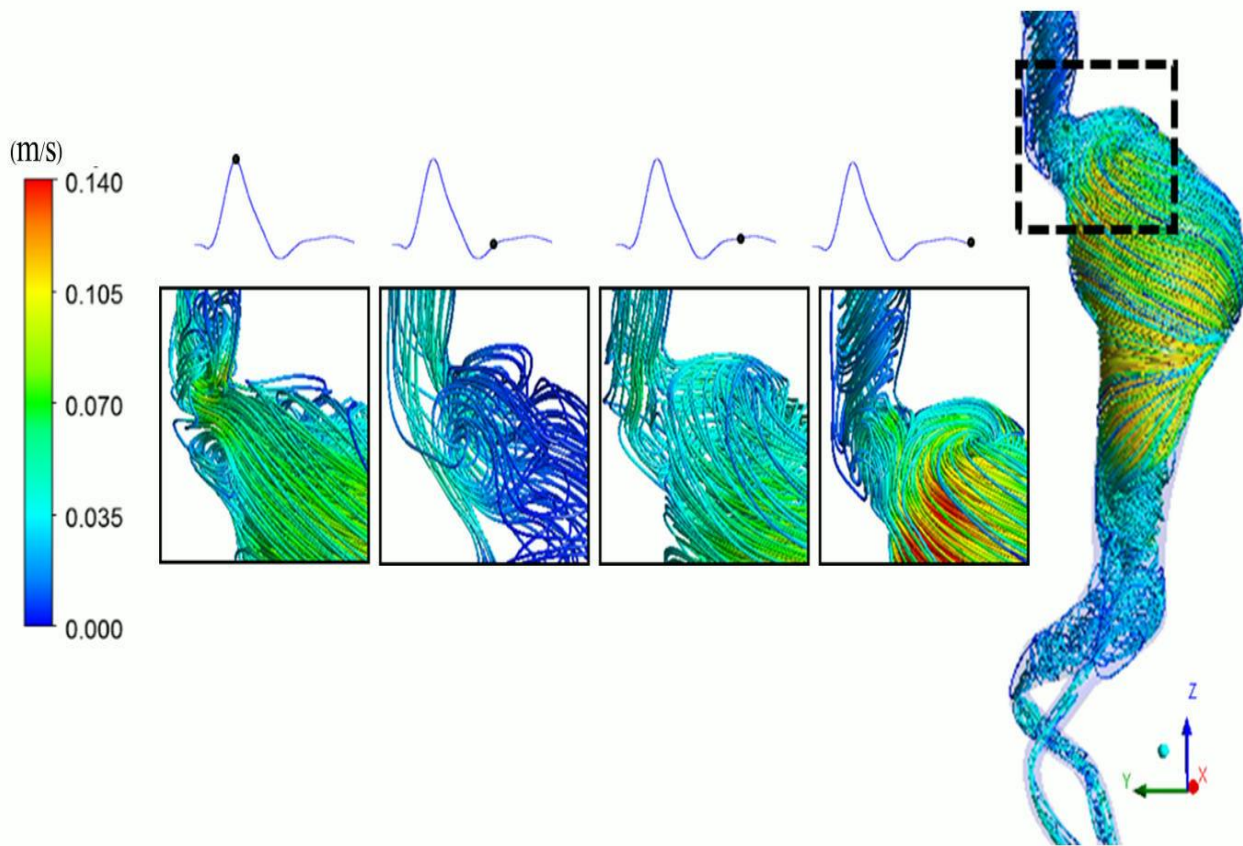
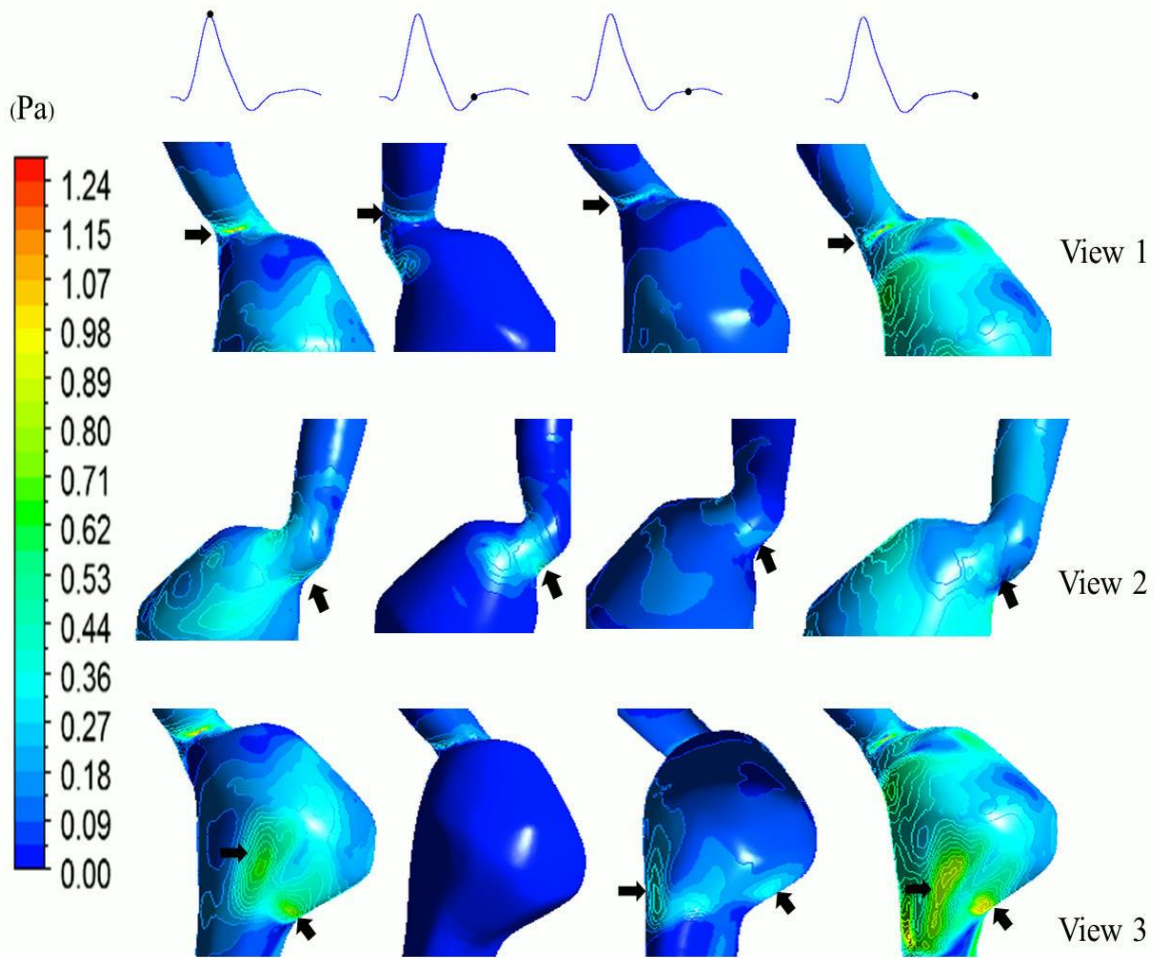Fig. 4: Flow streamline contours at four different time points in a cardiac cycle.

Fig. 5: WSS distribution on the angular neck and aneurysm sac regions at different time-points in a cardiac cycle.
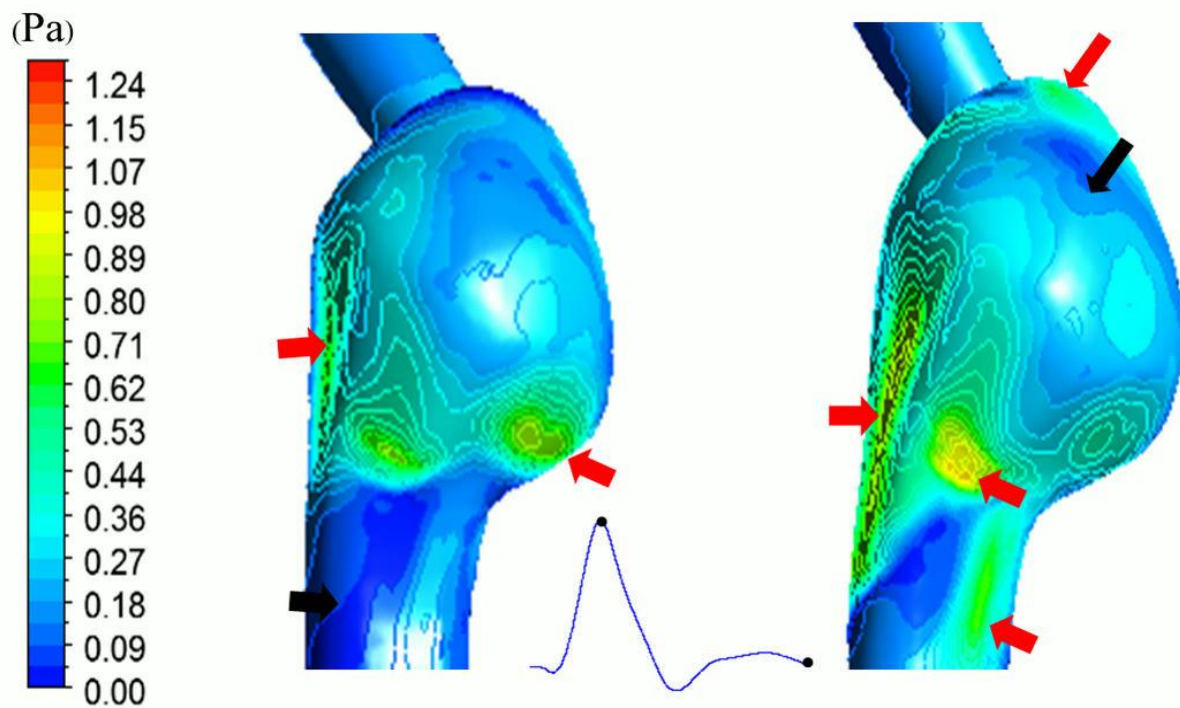
Fig.6: WSS distribution for two time-points in a cardiac cycle as prescribed by the graph. The high WSS regions are located with red arrows with average value of 0.94 Pa, while the locations of low WSS with the average of 0.077 Pa are indicated by the black arrows.

Y A Algabri[1], S Rookkapan[2] and S Chatpun[1]
[1]Institute of Biomedical Engineering, Faculty of Medicine, Prince of Songkla University, Hat Yai, Songkhla, Thailand
[2]Department of Radiology, Faculty of Medicine, Prince of Songkla University, Hat Yai, Songkhla, Thailand

E-mail: algabriyousif80@gmail.com

Paper ID	Track	Title
13-458	Track 1	THREE-DIMENSIONAL FINITE VOLUME MODELLING OF BLOOD FLOW IN SIMULATED ANGULAR NECK ABDOMINAL AORTIC ANEURYSM

| Abstract | An abdominal aortic aneurysm (AAA) is considered a deadly cardiovascular disease that defined as a focal dilation of blood artery. The healthy aorta size is between 15 and 24 mm based on gender, body weight, and age. When the diameter increased to 30 mm or more, the rupture can occur if it is kept growing or untreated. Moreover, the proximal angular neck of aneurysm is categorized as a significant morphological feature with prime harmful effects on endovascular aneurysm repair (EVAR). Flow pattern in pathological vessel can influence the vascular intervention. The aim of this study is to investigate the blood flow behaviors in angular neck abdominal aortic aneurysm with simulated geometry based on patient's information using computational fluid dynamics (CFD). The 3D angular neck AAA models have been designed by using SolidWorks Software. Consequently, CFD tools are used for simulating these 3D models of angular neck AAA in ANSYS FLUENT Software. Eventually, based on the results, we summarized that the CFD techniques have shown high performance in explaining and investigating the flow patterns for angular neck abdominal aortic aneurysm. |

PAPER • OPEN ACCESS

Three-dimensional finite volume modelling of blood flow in simulated angular neck abdominal aortic aneurysm

To cite this article: Y A Algabri *et al* 2017 *IOP Conf. Ser.: Mater. Sci. Eng.* **243** 012003

View the article online for updates and enhancements.

Related content

- Hemodynamics altered by placing helix stents in an aneurysm
  Tong-Miin Liou, Yi-Chen Li and Te-Chuan Wang

- Effect of aorto-iliac bifurcation and iliac stenosis on flow dynamics in an abdominal aortic aneurysm
  Shivam Patel, Abdullah Y Usmani and K Muralidhar

- Development of a custom-designed echo particle image velocimetry system
  Lingli Liu, Hairong Zheng, Logan Williams et al.

Three-dimensional finite volume modelling of blood flow in simulated angular neck abdominal aortic aneurysm

Y A Algabri[1], S Rookkapan[2] and S Chatpun[1]

[1]Institute of Biomedical Engineering, Faculty of Medicine, Prince of Songkla University, Hat Yai, Songkhla, Thailand
[2]Department of Radiology, Faculty of Medicine, Prince of Songkla University, Hat Yai, Songkhla, Thailand

E-mail: algabriyousif80@gmail.com

Abstract. An abdominal aortic aneurysm (AAA) is considered a deadly cardiovascular disease that defined as a focal dilation of blood artery. The healthy aorta size is between 15 and 24 mm based on gender, bodyweight, and age. When the diameter increased to 30 mm or more, the rupture can occur if it is kept growing or untreated. Moreover, the proximal angular neck of aneurysm is categorized as a significant morphological feature with prime harmful effects on endovascular aneurysm repair (EVAR). Flow pattern in pathological vessel can influence the vascular intervention. The aim of this study is to investigate the blood flow behaviours in angular neck abdominal aortic aneurysm with simulated geometry based on patient's information using computational fluid dynamics (CFD). The 3D angular neck AAA models have been designed by using SolidWorks Software. Consequently, CFD tools are used for simulating these 3D models of angular neck AAA in ANSYS FLUENT Software. Eventually, based on the results, we summarized that the CFD techniques have shown high performance in explaining and investigating the flow patterns for angular neck abdominal aortic aneurysm.

1. Introduction

Aneurysm is an enlargement or dilation of vessels, in another word, a bulging or ballooning the wall of blood vessel [1]. The aortic aneurysm is commonly occurring at the region of thoracic, thoracoabdominal, and abdominal [2]. Abdominal aortic aneurysm (AAA) forms and grows in the abdominal aorta which usually located between the renal arteries and the iliac bifurcation in the infrarenal abdominal aorta [1]. The healthy abdominal aorta diameter is between 15 and 24 mm in humans based on gender, body weight, and age. The aneurysm results in aorta dilation, typically 50 % greater than the normal diameter of healthy abdominal aorta [3]. There are several symptoms that accompany the aneurysm rupture such as sudden abdomen or back pain, sever dizziness, clammy and wet skin, and rapidity of heart rates [3]. The aneurysm rupture is a serious illness with 65% to 85% rate of mortality in many cases where almost half of death cases happened before admitting to the surgery. About 1.3% of deaths amongst men between 60 - 85 years old caused by AAA in developed countries while in USA is considered as 13th of deaths leading cause [3]. Moreover, in Netherlands's hospitals for period between 1972 and 1992, there were obvious increases of AAA patients due to the detection improvement in ultrasound [4]. Therefore, in many developed countries health care reported this aneurysm is a major health problem. Therefore, it is significant for aneurysm to be treated when it is found before gradually increase widening. Furthermore, endovascular aneurysm repair (EVAR) is considered a less invasive surgical procedure and has become a preferable treatment for many eligible

patients due to minor preoperative risks, lesser mortality, and long-term healing just like open surgery [5,6]. However, some of those eligible patients are not accepted for the EVAR procedure treatment. Due to complicated morphological aneurysm for example short aortic angular neck or highly proximal aortic angulated neck [7]. Shortly, there are few points to be considered when we study on neck angulations of AAA and their measurements such as knowing the exact location where angle occurs, the angle of neck formed in the area beneath the renal artery, proximal neck of an aneurysm and the bifurcation aorta. In contrast, the ideal neck angle of aorta is to be less than 60° if the angle is greater than that it leads to some implantation difficulties, endoleak and as well as the possibility for distal device migration. Computational fluid dynamics (CFD) is increasingly used in cardiovascular medicine that can play an important role in investigating and solving various complicated physiological fluid flows and demonstrating their potentials [8]. The aim of this study is to use CFD technique to investigate the flow pattern in the simulated angular neck abdominal aortic aneurysm.

2. Materials and methods

2.1. Geometry
In this study, we used a geometry which was based on idealized fusiform angular neck abdominal aortic aneurysm (AAA) of patient. The 3-dimensional simulated geometry was constructed by using computer-aided software SolidWorks (Solid Works Corp, Concord, MA) as shown in figure 1. The aneurysm size of 55 mm represented an average risk of rupture [9, 10]. Therefore, the four geometries were designed with the same concepts but the only difference was the neck angle (θ) of aneurysm which was technically set with an increment of 10 degrees as 60°, 70°, 80° and 90° [2].
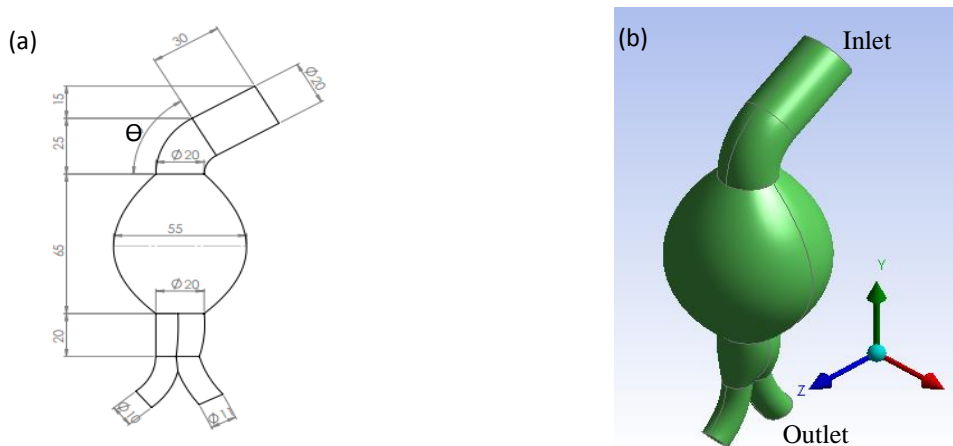

Figure 1. (a) Angular neck AAA simulated geometry and (b) 3-dimensional model

2.2. Meshing
The four-idealized angular neck AAA geometries were computationally meshed by using ANSYS FLUENT v16.2 (ANSYS Inc., Canonsburg, PA, USA). Tetrahedral meshing and a minimum of 1 mm body element size were applied. Cyclic quality checking and smoothing were done to reach satisfying mesh quality. Five different element numbers were used to determine the mesh quality were 55,304, 71,379, 391,306, 972,832 and 1,029,702. The blood properties and steady-state boundary conditions were applied for all mesh independency simulations. As shown in figure 2, the maximum velocity tended to be plateau when increasing the numbers of elements which indicated for velocity convergence and mesh independence.
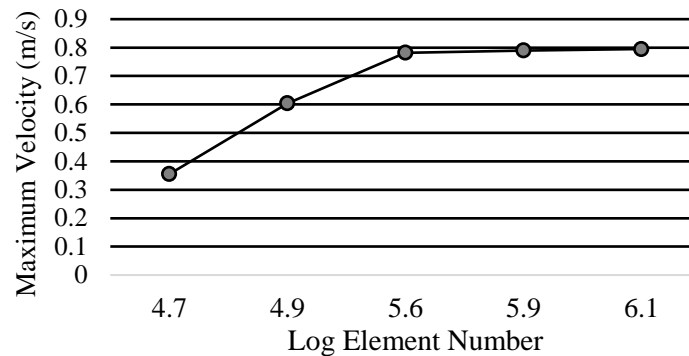
Figure 2. Mesh independence test based on maximum velocity

2.3. Governing equations

The fluid model solved numerically based on 3-dimensional incompressible Navier-Stokes equations along with the equations of momentum conservation (1) and mass conservation (2).

$$\rho \left(\frac{\partial u}{\partial t} \right) + \rho (u \cdot \nabla) u = -\nabla P + \mu \nabla^2 u, \tag{1}$$

$$\nabla \cdot (u) = 0, \tag{2}$$

where u, P, ρ, μ, and ∇ represent velocity, pressure, density, dynamic viscosity, and gradient symbol, respectively.

2.4 Simulation setup

The blood flow through the aorta was assumed to be incompressible and Newtonian fluid [8, 11]. The density and dynamic viscosity were considered constant with value of 1,060 kg/m^3 and 0.0035 Pa·S, respectively [12]. This viscosity was at approximately 45% of hematocrit value [13]. For all models, the steady-state simulation was performed with an inlet velocity of 0.28 m/s and outlet pressure of zero as well as the aortic wall was assumed to be no-slip and rigid [14]. The Reynolds number at the aorta inlet was calculated as of 1,696 based on inlet velocity and inlet aorta diameter, so flow was treated as laminar model. The CFD simulations were solved by using a commercial finite volume solver, ANSYS FLUENT v16.2 (ANSYS Inc., Canonsburg, PA, USA). All simulations were conducted on workplace computer with 3.40 GHz quad-core processor with 16.0 GB RAM.

3. Results and discussion

3.1. Flow behaviors at proximal aneurysm neck angulation

The flow patterns in angular neck and aneurysm sac were presented as velocity contours with more details in three different areas. The velocity contours on horizontal cross-sectional ZX-plane for the location below proximal aortic aneurysm neck is presented as in figure 3(a)**.** The volume of blood flow was forming a half circular shape of velocity contour with low velocity in angular neck 60 and 70 degrees. Furthermore, it is observed that when the degree of angular neck increases, the velocity gradually increases in the centre of aorta. The chart in figure 3(b) shows the increment of average velocity in the four aortic neck angulations.
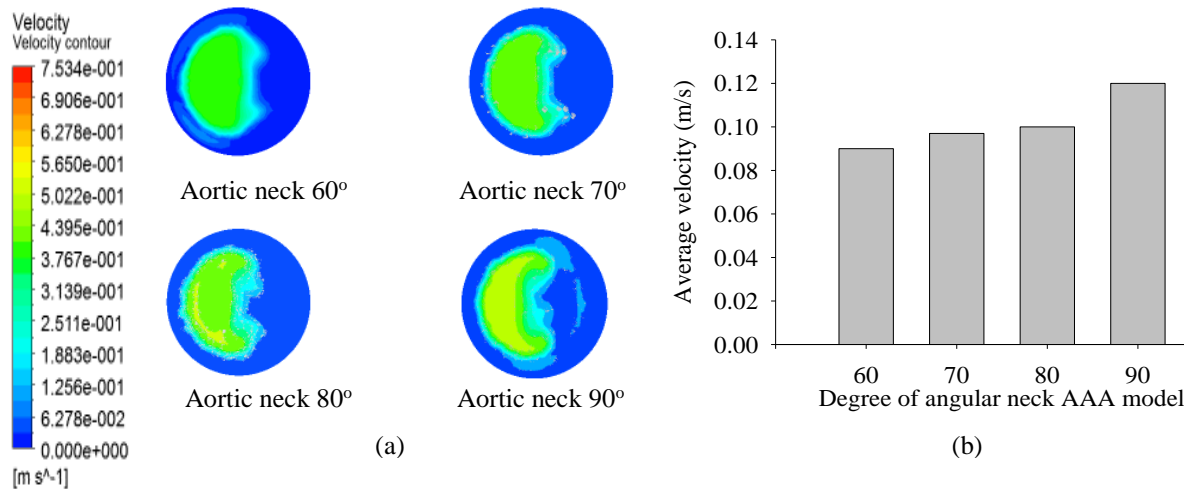
Figure 3. (a) Velocity contours at proximal neck of aneurysm sac, (b) average velocity at each neck at ZX-plane

However, to predict the exact change of velocity flow fields at the neck, the reference points were given at proximal aneurysm sac as revealed in figure 4(a) for this purpose. The average velocity values obtained by using the points starting from the near inner wall of the neck and reach to the outer wall of aneurysm are plotted in figure 4(b). It is clearly demonstrated that the velocity rose until it reached maximum value about 0.4 m/s and kept in the same range in the central region of aortic neck with little increase in 80° and 90° angles before it dropped to initial value zero at the outer wall of the distal neck.
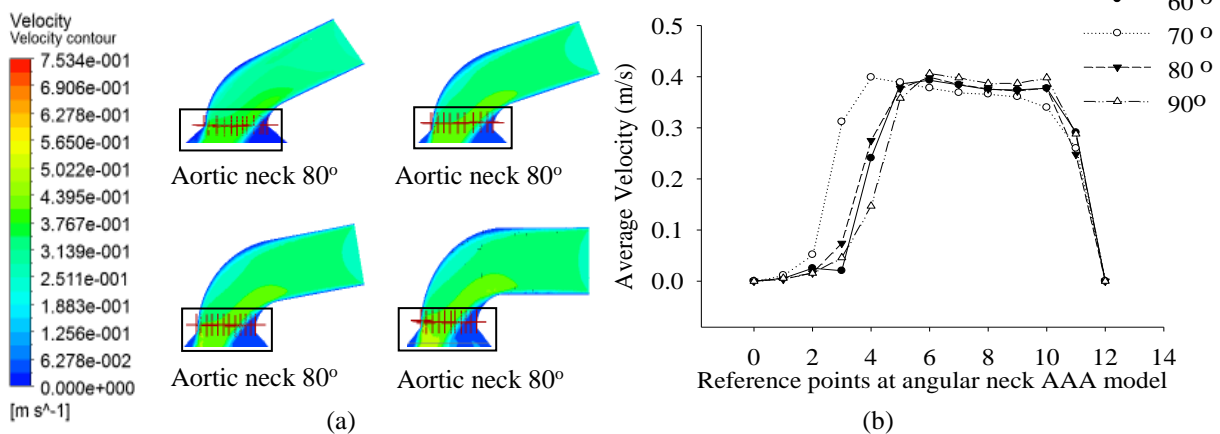

Figure 4. (a) 12-Point regions indicated by boxes in 4 geometries, (b) velocity values at 10-Points in angular neck AAA. On the X-axis, point 0 represents inner wall and point 12 represents outer wall.

3.2. Flow pattern through angular neck AAA model
The flow as illustrated in figure 5 on the longitudinal cross-section YZ-plane presents a fluffy bar of velocity from the proximal aneurysm neck cross the aneurysm sac towards the distal region of abdominal aortic aneurysm. At the same time, the velocity contours showed that the thin strip of high velocity is increasing gradually in the four angular neck aortas based on the change of degree of angular neck AAA.
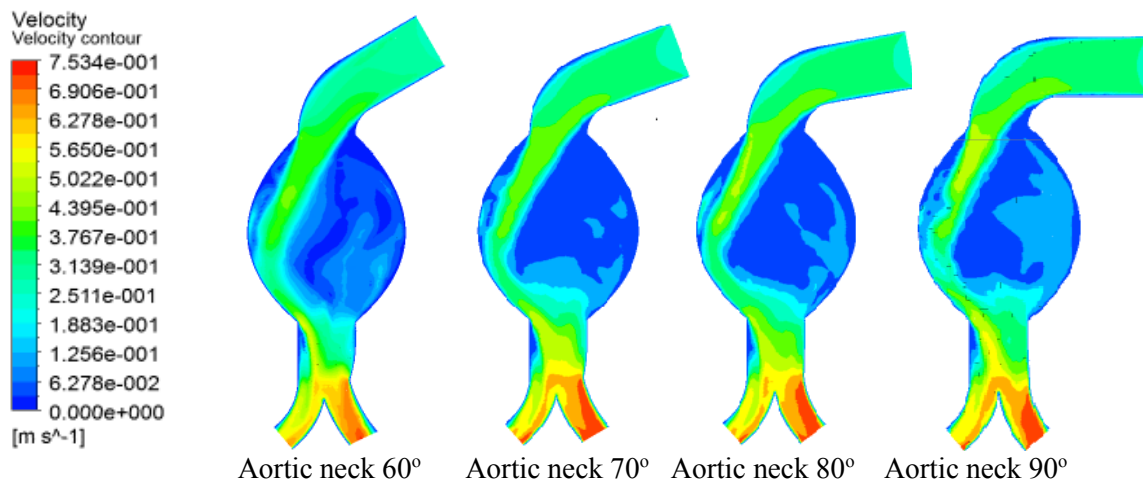
Figure 5. Velocity contours at the longitudinal YZ-plane of the angular neck AAA
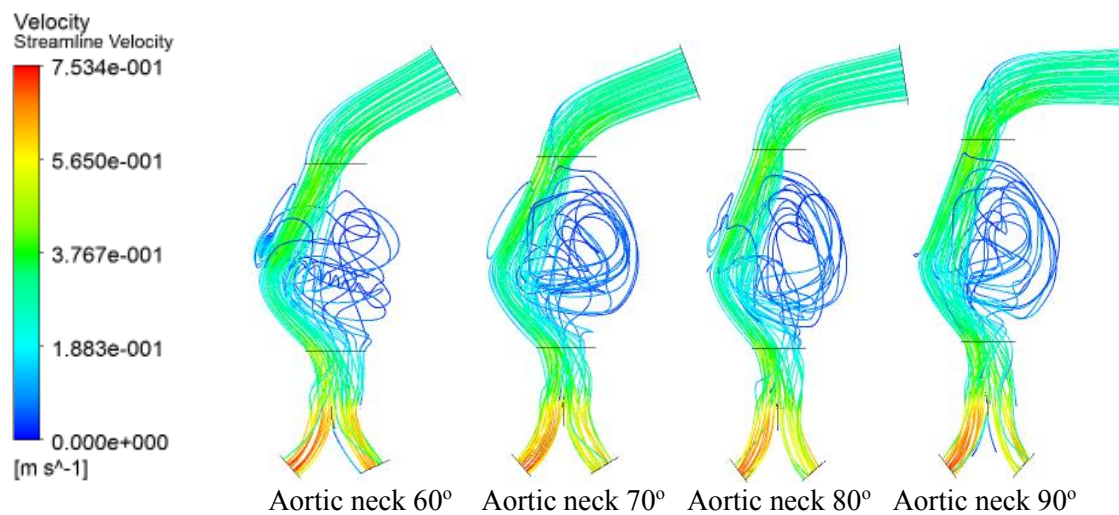

Figure 6. Velocity streamlines of angular neck AAA

The velocity streamlines are presented in Figure 6. The different recirculation vortexes were detected at the aneurysm in all aortic angular neck. However, when the angular neck of aorta rises, it is observed that the pattern of vortex inside aneurysm sac is debilitated and the velocity field appears to be more intensive near the middle of aorta.

Even though, this simulation was performed with idealized fusiform models but the simulation was based on realistic patient's information [15]. As findings in our study, the numerical simulation of the four geometries of highly angular neck AAA using computational fluid dynamics (CFD) has confirmed that the significant influence of aortic neck angles on the velocity flow field because of the degree of angular neck change impacts on the flow downstream [2]. Moreover, we calculated the flow rate ($Q = v_{ave} \cdot A$) at the left and right iliac outlets as shown in figure 7(a) based on the average velocity (v_{ave}) at the outlets and the cross-sectional area (A) of each iliac aorta. Since the inlets and outlets of the simulated angular neck AAA geometries were the same with the value of each outlet (left iliac = 11 mm and right iliac = 10 mm), the cross-sectional area of outlet was $A_{left\ iliac} \cong 9.5 \times 10^{-5} m^2$ and $A_{right\ iliac} \cong 7.85 \times 10^{-5} m^2$. The average velocity values for all angular neck AAA models at both outlets were

presented in table 1. It was found that the average velocity at the left iliac outlet was higher than the average velocity at the right iliac outlet. The plotted chart in figure 7(b) illustrated the difference of flow rates at the outlet of each iliac aorta for each degree of angular neck AAA model. Although, the difference was as shown very minimum but we still can observe the influence of angular neck degrees on the flow rates at the outlet regions for each model. Eventually, it is proper to mention that the findings of this study have some limitations because it was performed under steady-state fluid flow condition, while the blood naturally is transient flow.
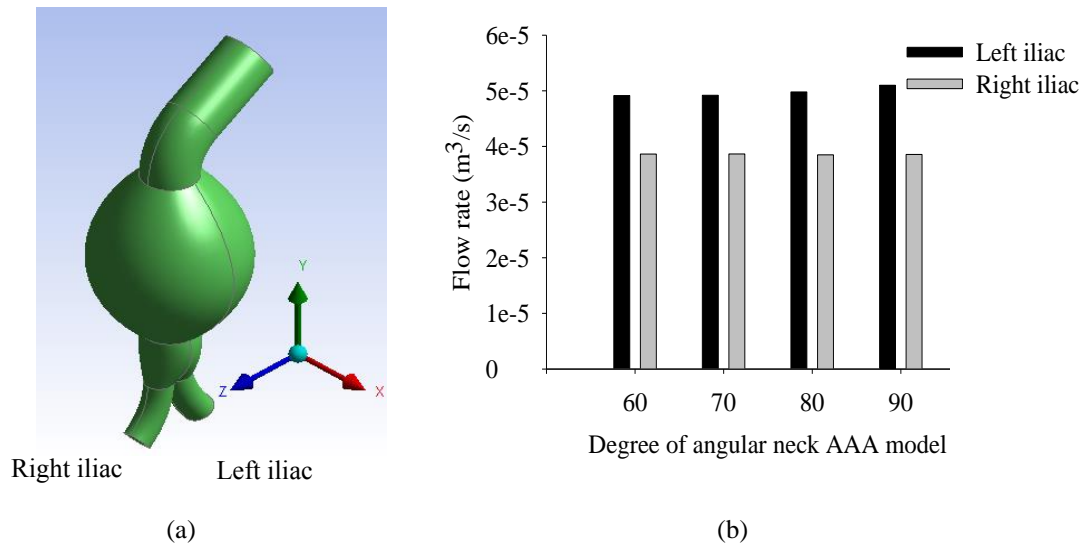

Right iliac   Left iliac

(a)   (b)

Figure 7. (a)Three dimensional model and (b) Flow rate at each iliac aorta outlet

Table 1. Average velocity values at both iliac aorta outlets.

Neck	Average velocity (m/s)	
	Left iliac outlet	Right iliac outlet
60°	0.5171	0.4921
70°	0.5176	0.4923
80°	0.5239	0.4904
90°	0.5271	0.4913

4. Conclusion

Four angular neck abdominal aortic aneurysm (AAA) models were simulated by using CFD technique to explain blood flow behaviours. As the results, by applying the steady state and fluid conditions on the three-dimensional angular neck AAA models, we can foresee the behaviours of the blood flow through the angular neck, aneurysm sac and as well the flow rate at the iliac aortas. Moreover, the study found that there was a correlation between the degrees of angular neck AAA and the pattern of the blood flow through the aorta. Therefore, the three-dimensional finite volume modelling and CFD technique can provide better visual details for blood flow in cardiovascular system which is useful for the cardiovascular intervention.

References
[1]   Kruchten T Van 2015 (Delft: Delft   University of Technology)
[2]   Yeow S L and Leo H L 2016 *Comput. Math. Methods. Med* **2016** 3830123
[3]   Sakalihasan N, Limet R and Defawe O 2005 *Lancet*. **365** 1577-89
[4]   Reitsma JB, Pleumeekers H J C M, Hoes A W, Kleijnen J, De Groot R M, Jacobs M J, Grobbee D E and Tijssen J G P 1996 *Eur.J. Vasc. Endovasc.Surg*. **12** 446-51
[5]   Greenhalgh R M, Brown L C, Kwong G P, Powell J T and Thompson S G 2004 *Lancet*. **364** 843–848
[6]   Prinssen M, Verhoeven E L, Buth J, Cuypers P W, van Sambeek M R, Balm R and Blankensteijn J D 2004 *N. Engl. J. Med*. **351** 1607-1618
[7]   Morrison T M, Meyer C A, Fillinger M F, Fairman R M, Glickman M H, Cambria R P, Farber M A, Naslund T C, Fail P S, Elmore J R**,** White R A and Dall'Olmo C A and Williams D M 2013 *J. Vasc. Surg.* **57** 24S
[8]   Morris P D, Narracott A, von Tengg-Kobligk H, Soto D A S, Hsiao S, Lungu A, Evans P, Bressloff N W, Lawford P V, Hose D R and Gunn J P 2016 *Heart*. **102** 18-28
[9]   Meecham L, Evans R, Buxton P, Allingham K, Hughes M, Rajagopalan S, Fairhead J, Asquith J R and Pherwani A D 2015 *Eur.J. Vasc. Endovas*c. **49** 28-32
[10] Duncan J L, Harrild K A, Iversen L, Lee A J and Godden D J 2012 *BMJ* **2958** 1-9
[11] Shek T L, Leonard W T, Nabovati A and Amon C H 2012 *J. Biomech. Eng*. **134** 121002
[12] Frauenfelder T, Lotfey M, Boehm T and Wildermuth S 2006 *Cardiovasc. Intervent. Radiol*. **29** 613–23
[13] Carty G, Chatpun S and Espino D M 2016 *J. Med. Bio. Eng*. **36** 396–409
[14] Taylor T W and Yamaguchi T 1994 *J. Biomech. Eng*. **116** 87-97
[15] Li Z and Kleinstreuer C 2007 *Eur. J. Mech. B-Fluid*. **26** 615-631

Vitae

Name   Yousif Ali Yousif Al-Gabri
Student ID   5910320020
Educational Attainment

Degree	Name of Institution	Year of Graduation
Bachelor of Engineering (Honors) (Biomedical Electronic Engineering)	Universiti Malaysia Perlis	2015

Scholarship Awards during Enrolment
- Thailand's Education Hub for ASEAN Countries (THE-AC) scholarship award for Master's study year 2016-2017.
- Graduate School dissertation funding for thesis.

Other Awards during Study
- Best Conference Paper award, CFDRI 2017 International Conference, BP hotel, Songkhla, Thailand.
- A keynote speaker at CFDRI2017 International Conference, BP hotel, Songkhla, Thailand.
- 1st runner up award at 4th Joint Symposium BMS-BME-EU: Post-graduate Health Science and Technology Conference 2017, Faculty of Medicine, Prince of Songkla University, Thailand.

List of Publication and Proceeding
- Yousif A. Algabri, Sorracha Rookkapan, Vera Gramina, Daniel M. Espino, and Surapong Chatpun1. Computational study on hemodynamic changes in patient-specific proximal neck angulation of abdominal aortic aneurysm with time-varying velocity, (Submitted to Journal of Cardiovascular Translational Research).
- Yousif A. Algabri, S. Rookkapan, and S. Chatpun, "Three-dimensional finite volume modelling of blood flow in simulated angular neck abdominal aortic aneurysm", IOP Conf. Ser. Mater. Sci. Eng., Vol. 243, No. 1, 2017.
- Yousif A. Algabri, and K. S. Basaruddin, "Determination of Effective Elastic Properties of Vertebral Cancellous Bone Based on Image Grey Scale Value", Int. Conf. Power, Energy Commun. Syst. (IPECS 2015), 2015.